

Freeze-in and freeze-out of sterile neutrino dark matter

Rupert Coy^{1,*} and Michael A. Schmidt^{2,†}

¹*Service de Physique Théorique, Université Libre de Bruxelles,*

Boulevard du Triomphe, CP225, 1050 Brussels, Belgium

²*Sydney Consortium for Particle Physics and Cosmology,*

School of Physics, The University of New South Wales,

Sydney, New South Wales 2052, Australia

Abstract

A sterile neutrino with a keV-scale mass is a compelling dark matter candidate. We propose a new production mechanism involving the decay and annihilation of a complex scalar singlet with a Higgs portal coupling which develops a vacuum expectation value. The interactions of the resulting pseudo Nambu-Goldstone boson may thermalise the dark sector. We determine the region of parameter space where dark sector thermalisation is reached and discuss the most relevant cosmological observables. The scenario can be considered as the combination of a freeze-in of the dark sector followed by relativistic freeze-out.

* e-mail: rupert.coy@ulb.be

† e-mail: m.schmidt@unsw.edu.au

CONTENTS

I. Introduction	3
II. The model	5
III. Sterile neutrino production and free-streaming horizon	9
A. Contribution to N_{eff}	11
B. Sterile neutrino free-streaming horizon	11
IV. Heating of the ϕ bath: Calculation of T_ϕ	12
A. Higgs decays	13
B. SM SM $\rightarrow \varphi\varphi$ scattering	13
C. $hh \rightarrow \varphi$ inverse decay	15
D. Remarks on the dark sector temperature ratio z	16
V. Thermalisation of the ϕ bath	17
A. Initial ϕ thermalisation	19
B. Continued ϕ thermalisation	21
C. Discussion	21
VI. Thermalisation of sterile neutrinos	24
A. Initial sterile neutrino thermalisation	26
B. Continued sterile neutrino thermalisation	27
C. Discussion	27
VII. Conclusions	30
Appendices	31
A. Self energy of the pNGB	31
B. $\alpha\varphi \rightarrow \alpha\varphi$ scattering	33
References	35

I. INTRODUCTION

Although the Standard Model (SM) is a very successful model of nature, it remains incomplete. Notably, both the nature of dark matter (DM), which accounts for one quarter of the energy density of the Universe [1], and the origin of neutrino masses are unknown. The simplest explanation of the former is in terms of a new particle which is stable on cosmological timescales, interacts at most weakly with known baryonic matter, and is cold. Neutrinos themselves were one of the early dark matter candidates, but have long since been ruled out because their contribution to the Universe’s energy density is much too small and their lightness contradicts our understanding of large scale structure formation. An intriguing possibility for dark matter, however, is that it is comprised of sterile neutrinos with keV-scale mass [2], thereby linking DM to the neutrino mass problem.

Right-handed sterile neutrinos are a natural extension of the SM from a theoretical point of view, as they serve as the missing right-handed partners of the left-handed active neutrinos, moreover they can explain tiny neutrino masses through the seesaw mechanism [3–6]. Three right-handed neutrinos are sufficient for simultaneously describing dark matter, via a single keV-scale sterile neutrino, and generating neutrino masses, via two heavy sterile neutrinos [7]. Sterile neutrinos with a keV-scale mass are generally warm dark matter candidates (WDM) which suppress power at small scales and therefore may play some role in resolving small scale structure issues, although explanations involving baryonic physics or self-interacting DM have been more favoured recently [8]. Sterile neutrino DM with 7.1 keV mass has also been suggested as a possible explanation of the 3.55 keV x-ray line [9, 10]. More generally, the keV scale is an intriguing frontier to consider because both the Tremaine-Gunn bound [11] and Lyman- α data [12] forbid fermionic DM from being lighter than $\mathcal{O}(\text{keV})$.

Such light DM cannot be frozen out by electroweak interactions, because in that case it would be overabundant [13]. A simple, viable production mechanism for keV-scale DM is freeze-in [14, 15], where its abundance is initially negligible and is slowly produced via decay, annihilation or mixing controlled by a small coupling. In the presence of active-sterile neutrino mixing, sterile neutrinos are most straightforwardly produced via neutrino oscillations [2, 16, 17]. However, non-resonant neutrino oscillations has already been ruled out as the source of the overall DM abundance due to a combination of x-ray and Ly- α constraints [18]. Even in presence of a large lepton asymmetry, resonant neutrino oscillations [19] are still strongly restricted by Ly- α data [12].

A minimal extension of this scenario involves the production of sterile neutrinos from scalar

boson decay [20–31]. Within this, we will consider the possibility that the scalar is itself frozen-in [25, 27–29, 31], thus production is a two-step process. Initially, the scalar boson is produced; subsequently, it decays to sterile neutrinos. Existing studies have focused only on a real scalar field which is odd under a \mathbb{Z}_2 symmetry. After spontaneous symmetry breaking of the discrete symmetry, the scalar boson develops a vacuum expectation value and generates the sterile neutrino mass. Thus, the coupling controlling the scalar decay to sterile neutrinos is directly proportional to the sterile neutrino mass. The interactions of the sterile neutrinos (and often of the frozen-in scalar) are feeble enough that they do not thermalise. However, the breaking of the global discrete \mathbb{Z}_2 symmetry can lead to the formation of domain walls [32], which is an intrinsic problem of this real scalar singlet model.

In this work we propose an elegant way to avoid domain walls by promoting the discrete \mathbb{Z}_2 symmetry to a global $U(1)$ symmetry, and study its phenomenological implications. It requires the introduction of a complex scalar field, rather than a real scalar, to generate a sterile neutrino mass term after spontaneous symmetry breaking. This small change drastically modifies the phenomenology of sterile neutrino production in the early Universe. Interactions involving the pseudo Nambu-Goldstone boson (pNGB) can enable the frozen-in scalar sector to reach both chemical and kinetic equilibrium and thus to thermalise with a temperature $T_\phi < T$ (the model is therefore a concrete example of thermal DM with $T_\phi \neq T$, which was recently classified in [33]). It may even bring the sterile neutrinos into kinetic (and chemical) equilibrium. Since the interactions eventually go out of equilibrium and the sterile neutrino comoving number density becomes fixed at some temperature below the heavy scalar mass, it can be said to freeze-in and freeze-out.

This scenario is a departure from the usual case, as generally neither kinetic nor chemical equilibrium is reached for frozen-in fields which explain the observed dark matter abundance. In this work, we also include quantum statistical factors and apply the full relativistic treatment, making approximations where applicable. This is important in the context of the light sterile neutrino and pNGB.

The paper is organised as follows. In Sec. II we outline the production mechanism in general terms and introduce the model. Sterile neutrino production is discussed in Sec. III, and the temperature of the dark sector is computed in Sec. IV. The thermalisation of the scalar sector is addressed in Sec. V, and the thermalisation of the sterile neutrinos in Sec. VI. Finally, we discuss the results and conclude in Sec. VII. In the appendices we present some technical details related to scattering in the scalar sector.

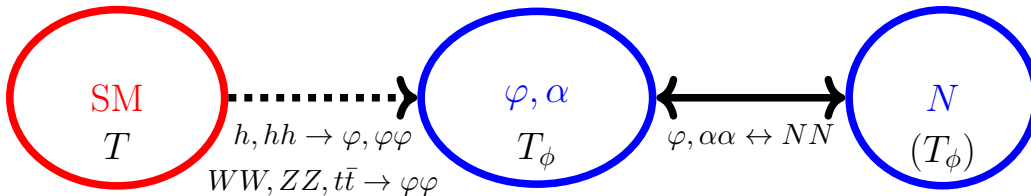


FIG. 1. Different sectors and the relevant interactions. The SM- ϕ interactions do not thermalise, but the ϕ sector self-scattering leads to thermal equilibrium such that the hidden sector develops a temperature $T_\phi < T$. The ϕ -N interactions may or may not thermalise the N population to the same temperature T_ϕ .

II. THE MODEL

The freeze-in mechanism [14, 15] is now a well-known scenario for the production of particles whose initial abundance is assumed to be negligible, possibly due to the inflationary dynamics.¹ A key feature of this mechanism is that interactions between the frozen-in particles and the thermal bath of SM particles (which has temperature T) is sufficiently feeble that the former never equilibrate with the latter. This feeble interaction is due to a very small coupling between the two sectors, which can nevertheless be technically natural [35]. The production predominantly takes place at temperatures of the order of the masses of the parent particles, as long as the interactions are renormalisable.

The mechanism we consider in this paper is schematically illustrated in Fig. 1. It involves a second iteration of the freeze-in scenario.² A complex scalar ϕ (which consists of a heavy scalar φ and pNGB α , see Eqn. (3)) and sterile neutrino N both have negligible initial abundance. First, φ is frozen-in via the decay or annihilation of particles in the thermal plasma. The ϕ itself equilibrates through self-interactions, forming its own thermal bath of φ and α with some temperature $T_\phi < T$. Note that models with only a real scalar typically do not thermalise [37], although there are exceptions, e.g. [31]. The presence of the pNGB component of the complex scalar enables rapid kinetic and chemical equilibration, which is a distinguishing feature between models with a real scalar and a complex one. In this work, we entirely focus on the region in parameter space where thermalisation is obtained. The relevant conditions for achieving thermalisation for the dark scalar sector are discussed in Secs. V and VI. We may describe ϕ in terms of its components φ and α as long as $T_\phi \lesssim T_{\phi,c}$, the critical temperature for the dark sector phase transition. Before the dark sector phase transition, the scalar is described as one

¹The impact of a non-negligible initial dark sector abundance was recently studied in [34].

²The scenario of successive freeze-in processes, i.e. $A \rightarrow B$ via freeze-in and then $B \rightarrow C$ also via freeze-in, where C is the DM, is called ‘sequential freeze-in’ in [36], see their Sec. VI for a related model.

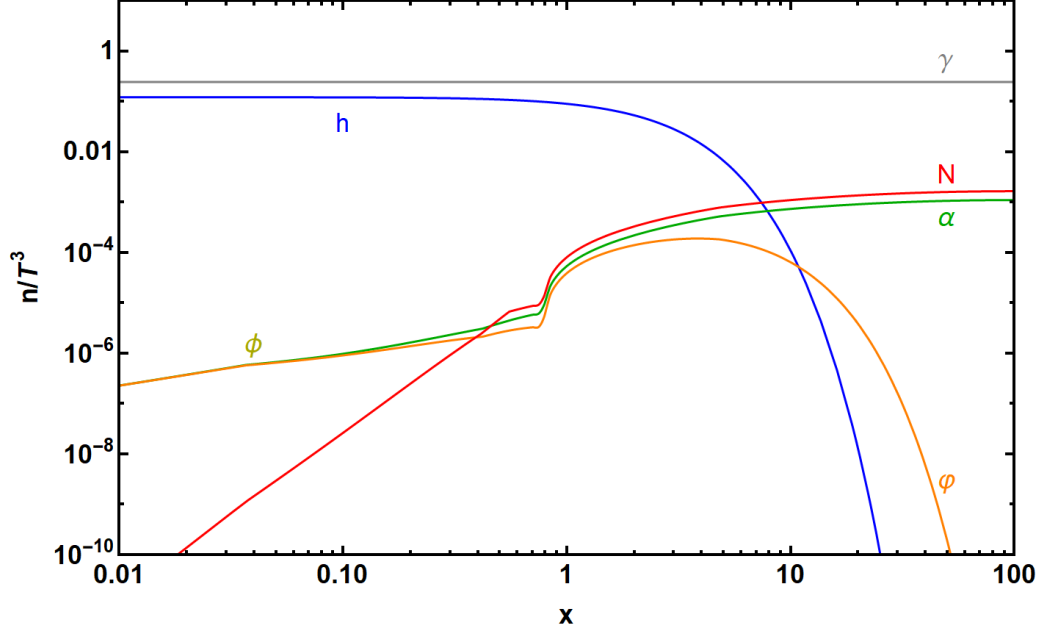


FIG. 2. Schematic plot of the particle number evolution, in terms of $x = m_h/T$. Here $m_\phi = 10$ GeV, $m_N = 10$ keV, $\lambda_\phi = 1$, while $\kappa = 5.3 \times 10^{-9}$ is fixed to ensure that sterile neutrinos give the correct DM relic abundance. The grey, blue, red, green and orange lines correspond to the photon, Higgs, sterile neutrino, α and ϕ number densities rescaled by T^3 . Early on $T_\phi > T_{\phi,c}$, thus there is a single number density of the complex scalar ϕ . The rapid increase in the N , α and ϕ number densities at $x \simeq 0.8$ is due to ϕ production from Higgs decays after the EW phase transition, see the text.

complex scalar field ϕ .

When $T_\phi \sim m_\phi$, the N population freezes in mainly from decays of the scalar ϕ , whose population then becomes Boltzmann suppressed, and annihilations of the α . Here, we consider the case where the N population eventually thermalises with the ϕ bath and thus is also described by temperature T_ϕ . However, we note that it is possible that the N population never thermalises, as we discuss in Sec. VI. The behaviour of the different sectors is outlined in Fig. 2.

In our explicit realisation of the mechanism we introduce in the theory a complex scalar singlet, ϕ , and a light right-handed singlet fermion, N , with lepton number -2 and 1, respectively (the SM lepton doublet and singlet, L and e , have lepton number 1). The Lagrangian is

$$\mathcal{L} = \mathcal{L}_{SM} + \partial_\mu \phi^\dagger \partial^\mu \phi - V(H, \phi) + i\bar{N}\not{\partial}N - \frac{f}{2}(\phi N^T C N + \text{h.c.}) - (y_i H \bar{L}_i N + \text{h.c.}) , \quad (1)$$

where C denotes the charge conjugation matrix. The scalar potential is given by

$$V(H, \phi) = \lambda \left(H^\dagger H - \frac{v^2}{2} \right)^2 + \lambda_\phi \left(|\phi|^2 - \frac{v_\phi^2}{2} \right)^2 + \kappa \left(|\phi|^2 - \frac{v_\phi^2}{2} \right) \left(H^\dagger H - \frac{v^2}{2} \right) . \quad (2)$$

The scalar ϕ and the Higgs doublet H are decomposed as follows:³

$$\phi = \frac{v_\phi + \varphi}{\sqrt{2}} e^{i\alpha/v_\phi} \quad H = \begin{pmatrix} G^+ \\ \frac{v+h+iG^0}{\sqrt{2}} \end{pmatrix}, \quad (3)$$

with the electroweak VEV $v = (\sqrt{2}G_F)^{-1/2} \simeq 246$ GeV. The coupling f can be made real by a rotation of N , the sterile neutrino field. The Yukawa couplings, y_i , are generally complex in the presence of massive neutrinos and naturally small, $|y_i| \ll 1$, because the symmetry of the model is enhanced in their absence (in conjunction with $|\kappa| \ll 1$). Specifically, decoupled N and ϕ may transform under their own independent $U(1)_N$ symmetry with charges 1 and -2 , respectively. The active-sterile mixing angles are given by

$$\theta_i \sim \frac{y_i v}{m_N}, \quad (4)$$

with sterile neutrino mass given by

$$m_N = \frac{f v_\phi}{\sqrt{2}}. \quad (5)$$

Strict experimental constraints on θ_i mandate that the y_i are tiny. For instance, for $m_N = 7.1$ keV, x-ray bounds constrain $y_i \lesssim 10^{-13}$ [37], while sterile neutrino decays to an active neutrino and a Majoron pose an even stronger constraint, $y_i \lesssim 10^{-19}(10^{-6}/f)$. We thus take the limit of vanishing Yukawa couplings y_i in the following and work with the $U(1)_N$ symmetry instead of lepton number.

In Eqn. (1) we take $\kappa \ll 1$, its smallness is protected by an enhanced Poincaré symmetry in the limit that $\kappa \rightarrow 0$ (see [38]). The potential at zero temperature is minimised by the VEVs, v and v_ϕ . The VEV of ϕ breaks $U(1)_N$, giving mass to the sterile neutrino. As CP is conserved in the scalar sector, there is no mixing between the CP-even states φ , h and the CP-odd pNGB α . The mass matrix for h, φ is

$$M = \begin{pmatrix} 2\lambda v^2 & \kappa v v_\phi \\ \kappa v v_\phi & 2\lambda_\phi v_\phi^2 \end{pmatrix}. \quad (6)$$

The mixing of φ with the Higgs induces a coupling of two α particles with a pair of SM fermions, however this is suppressed by the small mixing. Since the off-diagonal elements are tiny due to the factor of κ , we have

$$m_h^2 \approx 2\lambda v^2 \quad \text{and} \quad m_\varphi^2 \approx 2\lambda_\phi v_\phi^2. \quad (7)$$

³We decomposed the complex scalar, ϕ , into modulus and phase, rather than real and imaginary parts. This simplifies calculations and makes the proportionality of matrix elements to the momenta of external pNGBs α explicit.

The first relation gives $\lambda \approx 0.129$ in order to explain the SM Higgs boson mass of $m_h = 125$ GeV. The CP-even scalar mass eigenstates (s_1, s_2) are

$$\begin{pmatrix} h \\ \varphi \end{pmatrix} = \begin{pmatrix} \cos \theta & -\sin \theta \\ \sin \theta & \cos \theta \end{pmatrix} \begin{pmatrix} s_1 \\ s_2 \end{pmatrix}, \quad (8)$$

with the mixing angle given by

$$\tan(2\theta) = \frac{vv_\phi\kappa}{\lambda v^2 - \lambda_\phi v_\phi^2} \approx \frac{2vv_\phi\kappa}{m_h^2 - m_\varphi^2}. \quad (9)$$

The last approximation holds as long as $m_h^2 - m_\varphi^2 \gg 4\kappa vv_\phi$, but breaks down when the scalar masses are almost degenerate. As the mixing angle is very small, we will neglect it except when it is important for a physical process like the production of the new scalars from Higgs decay or annihilation. In this limit, the relevant interactions of the CP-even scalars are

$$V \supset \lambda v s_1^3 + \lambda_\phi v_\phi s_2^3 + \kappa \frac{s_1^2 s_2^2}{4} + \kappa v \frac{2m_\varphi^2 + m_h^2}{m_h^2 - m_\varphi^2} \frac{s_1 s_2^2}{2} - \kappa v_\phi \frac{2m_h^2 + m_\varphi^2}{m_h^2 - m_\varphi^2} \frac{s_1^2 s_2}{2}. \quad (10)$$

In the following, we will simplify the notation and denote the mass eigenstates by the interaction eigenstate with the largest contribution, i.e.

$$s_1 \approx h \quad \text{and} \quad s_2 \approx \varphi. \quad (11)$$

The spontaneous breaking of the global $U(1)_N$ symmetry by the VEV of the ϕ leads to a pNGB, so α is (almost) massless even in the presence of thermal corrections due to the Goldstone theorem. The global $U(1)_N$ symmetry will generally be explicitly broken by quantum gravity effects and induce a tiny mass for the pNGB, which however we neglect in the following. Equally, the population of pNGBs produced in the early Universe via the misalignment mechanism is negligible in this scenario [39]. The VEVs depend on thermal corrections and become non-zero below the critical temperatures $T_{\text{ew},c} = 159.5 \pm 1.5$ GeV [40] in the SM sector and $T_{\phi,c} = \sqrt{3/(2\lambda_\phi)} m_\varphi$ in the dark sector. The dark sector generally has a lower temperature, T_ϕ , than the SM. We parameterise it in terms of the temperature ratio

$$z \equiv \frac{T_\phi}{T}. \quad (12)$$

Although there is generally a period in the cosmological evolution with $T_\phi > T_{\phi,c}$, it can often be neglected as long as the dominant production of dark sector particles occurs for $T \lesssim 12m_\varphi(0.1/z)/\sqrt{\lambda_\phi}$, with the temperature ratio $z \lesssim 0.1$ required for the correct DM abundance. In the following, we will approximate the VEV evolution with step-functions and neglect the

intermediate unbroken dark sector phase. We will justify this approximation at the relevant places of our analysis.

After the breaking of the $U(1)_N$, the Lagrangian (1) is given by

$$\begin{aligned} \mathcal{L} = & \mathcal{L}_{SM} + \frac{1}{2} \partial_\mu \varphi \partial^\mu \varphi - V(H, \varphi) + i \bar{N} \not{\partial} N + \frac{1}{2} \partial_\mu \alpha \partial^\mu \alpha + \left(\frac{\varphi}{v_\phi} + \frac{\varphi^2}{2v_\phi^2} \right) \partial_\mu \alpha \partial^\mu \alpha \\ & - \left(\frac{m_N}{2} + \frac{f}{2\sqrt{2}} \varphi \right) (e^{i\alpha(x)/v_\phi} N^T C N + \text{h.c.}) . \end{aligned} \quad (13)$$

For small field excitations of the pNGB field, the interactions with the fermionic SM singlet are given by⁴

$$\mathcal{L} \supset -\frac{f}{2\sqrt{2}} \left(v_\phi + \varphi - \frac{\alpha^2}{2v_\phi} \right) \bar{N}_M N_M - i \frac{f}{2\sqrt{2}} \left(\alpha + \frac{\alpha\varphi}{v_\phi} \right) \bar{N}_M \gamma_5 N_M + \mathcal{O} \left(\frac{\alpha/\varphi}{v_\phi} \right)^3 , \quad (14)$$

where we expressed the Lagrangian in terms of the Majorana fermion, $N_M = N + N^C$. In the following, we drop the subscript M to simplify the notation.

In total, there are four independent parameters relevant for sterile neutrino production in the early Universe, the four what we work with being κ , λ_ϕ , m_φ , and m_N . The VEV, v_ϕ , and the Yukawa coupling, f , are given by

$$v_\phi = \frac{m_\varphi}{\sqrt{2\lambda_\phi}} , \quad f = \frac{\sqrt{2}m_N}{v_\phi} = \frac{2\sqrt{\lambda_\phi}m_N}{m_\varphi} . \quad (15)$$

III. STERILE NEUTRINO PRODUCTION AND FREE-STREAMING HORIZON

As outlined in the previous section, the ϕ sector is frozen-in via Higgs portal interactions. The DM candidate, N , is then mainly produced via $\varphi \rightarrow NN$ decays and $\alpha\alpha \rightarrow NN$ annihilations, with a rate determined by the coupling $f \ll 1$. Scalar-pNGB scattering, $\alpha\varphi \rightarrow NN$, is suppressed compared to pNGB scattering for $T_\phi \ll m_\phi$, i.e. when φ is non-relativistic, while other processes are completely negligible since they are suppressed by additional powers of f . For large $T_\phi \gtrsim m_\varphi$, the decay and annihilation rates are comparable, however in the regime $T_\phi \ll m_\varphi$ the sterile neutrinos are dominantly produced via the annihilation process since the φ population is exponentially suppressed. We note that the relic abundance of N produced via resonant or non-resonant oscillations from active neutrinos is absent due to the imposed $U(1)_N$ symmetry.⁵

⁴The pNGB couplings are generally derivative couplings due to the shift-symmetry. This can be made explicit by a local field redefinition of the SM singlet $N(x) \rightarrow e^{-i\alpha(x)/2v_\phi} N$ and similarly for other fermion fields. The kinetic term then induces a derivative coupling of the pNGB. It can be rewritten on-shell using equations of motion such that the coupling to fermions is proportional to the fermion mass.

⁵Even if active-sterile neutrino mixing were allowed, the contribution would be subdominant due to the very small θ_i . Resonant production requires a large lepton asymmetry [19], which is not generated in our model.

Assuming that the dark sector particles φ , α and N are in thermal equilibrium (an assumption we will discuss in detail in Secs. V and VI), and neglecting inverse processes from the $\phi - N$ bath to the SM,⁶ the relevant Boltzmann equation for energy transfer from the SM to the dark sector is

$$\int \frac{d^3 p_\varphi}{(2\pi)^3} E_\varphi \frac{df_\varphi}{dt} + \int \frac{d^3 p_\alpha}{(2\pi)^3} p_\alpha \frac{df_\alpha}{dt} + \int \frac{d^3 p_N}{(2\pi)^3} E_N \frac{df_N}{dt} = \int \frac{d^3 p_\phi}{(2\pi)^3} E_\phi \sum_i S_{\phi,i} \mathcal{C}_{\phi,i}[\text{SM} \rightarrow \phi], \quad (16)$$

where $\sum_i S_{\phi,i} \mathcal{C}_{\phi,i}[\text{SM} \rightarrow \phi]$ refers schematically to the sum of all collision terms for the production of the ϕ sector and $S_{\phi,i}$ is the number of ϕ produced in the given process (note $S_{\phi,i}$ is negative if ϕ particles are destroyed). The collision term for a final state particle in a $2 \rightarrow 2$ process, $\mathcal{C}_a[ij \rightarrow ab]$, is

$$\mathcal{C}_a = \frac{1}{S} \frac{1}{2E_a} \int d\Pi_b \int d\Pi_i \int d\Pi_j (2\pi)^4 \delta^{(4)}(p_i + p_j - p_a - p_b) |\mathcal{M}(ij \rightarrow ab)|^2 f_i f_j (1 \pm f_a)(1 \pm f_b), \quad (17)$$

where S is the symmetry factor which accounts for the multiplicities in the initial and final states, and $d\Pi_X = g_X d^3 p_X / ((2\pi)^3 2E_X)$ denotes the integration over the phase space of particle X with g_X internal degrees of freedom. $|\mathcal{M}(ij \rightarrow ab)|^2$ is the squared matrix element averaged over initial and final state spins. The reverse process is written separately and enters the Boltzmann equation with a minus sign because particles are destroyed. The index of \mathcal{C} denotes the particle which is singled out in the Boltzmann equation. The assumption of kinetic equilibrium implies that the $\varphi \leftrightarrow \alpha$, $\varphi \leftrightarrow N$ and $\alpha \leftrightarrow N$ collision terms that should appear in the right-hand side of Eqn. (16) in fact cancel out, for instance

$$\int \frac{d^3 p_\varphi}{(2\pi)^3} E_\varphi \mathcal{C}_\varphi[\varphi \rightarrow \alpha\alpha] = 2 \int \frac{d^3 p_\alpha}{(2\pi)^3} p_\alpha \mathcal{C}_\alpha[\alpha\alpha \rightarrow \varphi] \quad (18)$$

$$2 \int \frac{d^3 p_\alpha}{(2\pi)^3} p_\alpha \mathcal{C}_\alpha[\alpha\alpha \rightarrow NN] = 2 \int \frac{d^3 p_N}{(2\pi)^3} E_N \mathcal{C}_N[NN \rightarrow \alpha\alpha]. \quad (19)$$

The sterile neutrino number density after it thermalises is

$$n_N = \frac{3\zeta(3)T_\phi^3}{2\pi^2}, \quad (20)$$

since it has a Fermi-Dirac (FD) distribution with temperature T_ϕ . The dark sector interactions will inevitably go out of equilibrium when $T_\phi \gg m_N$, thus the sterile neutrino maintains a relativistic number density. Its relic energy density is therefore given by

$$\Omega_N h^2 \simeq 0.3 \left(\frac{z}{0.1} \right)^3 \frac{m_N}{10 \text{ keV}}. \quad (21)$$

⁶This is motivated by the standard freeze-in assumption that the ϕ and N number densities are initially negligible [14, 15]. Even at late times, after a substantial population of ϕ or N has been frozen-in, we may continue to neglect these reverse processes because the ϕ and N abundances are much smaller than the populations of their parents since $T_\phi \ll T$.

The evolution of z with time will be computed in the following section. From Eqn. (21), we see that for a keV-scale sterile neutrino, $z \simeq 0.1$ at very late times generates the observed DM abundance, $\Omega_{\text{dm}} h^2 = 0.12$ [1]. We will find in Sec. IV that $z \propto \sqrt{\kappa}$ and is independent of m_N . Thus, the relation $\Omega_N h^2 \propto \kappa^{3/2} m_N$ removes one free parameter from the model if we insist on a relic sterile neutrino density in agreement with observations.

Strictly, T_ϕ is ill-defined after the $\phi - N$ bath goes out of equilibrium, and consequently z is also ill-defined. However, after decoupling the α and N free-stream with $p \propto a^{-1}$, so after the decoupling time, $t_{\phi, \text{dec}}$, we set $T_\phi(t) \equiv [a(t_{\phi, \text{dec}})/a(t)] T_\phi(t_{\phi, \text{dec}})$. In this case, the evolution of z after $t_{\phi, \text{dec}}$ is determined only by the number of relativistic SM degrees of freedom in entropy, g_*^S , and becomes constant after electron decoupling.

Finally, we note that in principle the pNGB α also contributes to the DM abundance due to its tiny mass, however this abundance is suppressed by a factor $\sim m_\alpha/m_N \ll 1$ compared to the sterile neutrino abundance and is therefore completely negligible.

A. Contribution to N_{eff}

There is a contribution to N_{eff} from both α and N , which is easily calculable in this scenario. Their energy density at $T_\phi \gg m_N$ is

$$\rho_{\text{dark}} = g_*^{\text{dark}} \frac{\pi^2 T_\phi^4}{30}, \quad (22)$$

where $g_*^{\text{dark}} = 11/4$. The value of N_{eff} at $T = 1$ MeV is therefore

$$N_{\text{eff}} = \rho_{\text{dark}} \left(\frac{7}{8} (4/11)^{4/3} \rho_\gamma \right)^{-1} \simeq 12.1 [z(1 \text{ MeV})]^4. \quad (23)$$

Taking $z \lesssim 0.1$, as required for the correct relic abundance (cf. Eqn. (21)), leads to $N_{\text{eff}} \sim 10^{-3}$, too small to be detected even in the next generation of experiments [41], which have an expected sensitivity of $\sigma(N_{\text{eff}}) \simeq 0.02 - 0.03$.

B. Sterile neutrino free-streaming horizon

The average momentum of the sterile neutrinos, given its FD distribution, is

$$\langle p_N(T_\phi) \rangle = \frac{\int d^3 p f_N p}{\int d^3 p f_N} = 3.15 T_\phi. \quad (24)$$

We can estimate the temperature at which the sterile neutrinos become non-relativistic by $\langle p_N \rangle = m_N$, i.e. $T_{\phi, \text{nr}} = m_N/3.15$. We denote the corresponding time by t_{nr} . Then the free-streaming horizon is given by

$$\lambda_{FS} = \frac{\sqrt{t_{\text{nr}} t_{\text{eq}}}}{a_{\text{eq}}} \left(5 + \ln \frac{t_{\text{eq}}}{t_{\text{nr}}} \right) \simeq 366 \frac{z \text{ keV}}{m_N} \left(7.299 + \ln \frac{m_N}{z \text{ keV}} \right) \text{ kpc} , \quad (25)$$

following the calculation of Ref. [27], where $t_{\text{eq}} = 1.9 \times 10^{11} \text{ s}$ is the time at matter-radiation equality and $a_{\text{eq}} = 8.3 \times 10^{-5}$ is the corresponding scale factor. Bounds from Ly- α data set a lower limit of $m_{\text{DM}} \geq 5.3 \text{ keV}$ on early-decoupled fermionic DM [42], which can be converted into the constraint $\lambda_{FS} \lesssim 66 \text{ kpc}$. Indeed, the bound on the sterile neutrino mass is also $m_N \gtrsim 5.3 \text{ keV}$, because for a given value of m_N , producing the observed dark matter abundance fixes the temperature ratio z via Eqn. (21), and thus the free-streaming horizon. This lower limit is shown in Fig. 7.

IV. HEATING OF THE ϕ BATH: CALCULATION OF T_ϕ

In the previous section, we introduced the time-dependent temperature ratio, z , and showed that it should be $\mathcal{O}(0.1)$ for the correct sterile neutrino relic abundance. In this section, we compute this function explicitly by calculating the energy injection into the $\phi - N$ thermal bath. The integrated Boltzmann equation is

$$\frac{d\rho_{\text{dark}}}{dt} + 4H\rho_{\text{dark}} = \int \frac{d^3 p_\varphi}{(2\pi)^3} E_\varphi \sum_i S_{\varphi, i} \mathcal{C}_{\varphi, i} [\text{SM} \rightarrow \varphi] , \quad (26)$$

where i sums over all channels of φ production $\text{SM} \rightarrow \varphi$ (α production is subdominant, and recall that N are created from the ϕ sector). The energy density of the thermalised dark sector is given in Eqn. (22), where $g_*^{\text{dark}} = 15/4$ for $T_\phi \gg m_\varphi$ and $11/4$ for $T_\phi \ll m_\varphi$. Hence the left-hand side of Eqn. (26) is

$$\frac{d\rho_{\text{dark}}}{dt} + 4H\rho_{\text{dark}} = \frac{2\pi^2 g_*^{\text{dark}} m_h^6 H_* z^3}{15x^5} \frac{dz}{dx} , \quad (27)$$

where $H_* \equiv H/T^2$ and we parameterise time in terms of

$$x \equiv \frac{m_h}{T} . \quad (28)$$

Different channels of φ production are only kinematically allowed for certain values of m_φ . Combining Eqns. (26) and (27), we obtain

$$z(x) = \left[\int_0^x dx' \frac{30x'^5}{\pi^2 g_*^{\text{dark}} m_h^6 H_*} \left(\sum_i \int \frac{d^3 p_\varphi}{(2\pi)^3} E_\varphi S_{\varphi, i} \mathcal{C}_{\varphi, i} [\text{SM} \rightarrow \varphi] \right) \right]^{1/4} , \quad (29)$$

where we sum over the allowed processes and $S_{\varphi,i}$ denotes the number of φ particles produced in process i . We now compute these collision terms.

A. Higgs decays

For $m_\varphi < m_h/2$, Higgs decays dominate φ production. The integrated collision term is

$$2 \int \frac{d^3 p_\varphi}{(2\pi)^3} E_\varphi \mathcal{C}_\varphi[h \rightarrow \varphi\varphi] = m_h n_h^{eq} \Gamma(h \rightarrow \varphi\varphi) = \frac{\kappa^2 m_h^5 K_2(x)}{128\pi^3 \lambda x} \left(\frac{m_h^2 + 2m_\varphi^2}{m_h^2 - m_\varphi^2} \right)^2 \sqrt{1 - \frac{4m_\varphi^2}{m_h^2}}, \quad (30)$$

with

$$\Gamma(h \rightarrow \varphi\varphi) = \frac{\kappa^2 v^2}{32\pi m_h} \left(\frac{2m_\varphi^2 + m_h^2}{m_h^2 - m_\varphi^2} \right)^2 \sqrt{1 - \frac{4m_\varphi^2}{m_h^2}}. \quad (31)$$

In the limit that this decay is the only relevant process, combining Eqns. (29) and (30), gives

$$z(x) \simeq 0.018 \sqrt{\frac{\kappa}{10^{-10}} \frac{2m_\varphi^2 + m_h^2}{m_h^2 - m_\varphi^2}} \left(\frac{g_*^s}{100} \right)^{1/3} \left(\frac{100}{g_*^\rho} \right)^{1/8} \left(\frac{3.75}{g_{\text{dark}}^*} \right)^{1/4} \left(1 - \frac{4m_\varphi^2}{m_h^2} \right)^{1/8} \\ \times \left(\int_{x_{\text{ew,c}}}^x dx' x'^4 K_2(x') \right)^{1/4}, \quad (32)$$

where the integral's lower limit at $x_{\text{ew,c}} \equiv m_h/T_{\text{ew,c}} = 0.78$ reflects the electroweak phase transition, after which $h \rightarrow \varphi\varphi$ is allowed. The value of the integral at late times is $\int_{0.78}^\infty dx' x'^4 K_2(x') = 23.3$. Note that entropy dilution of the SM thermal plasma has explicitly been taken into account. We use the analytic expressions in the Appendix of [43] to trace the evolution of g_*^s and g_*^ρ accurately for our numerical results.

B. SM SM $\rightarrow \varphi\varphi$ scattering

For all values of m_φ , SM particles can scatter to produce pairs of φ . Before the electroweak phase transition, the cross section for the scattering of a Higgs doublet with its antiparticle to a particle-antiparticle pair of dark sector particles, $HH^* \rightarrow \phi\phi^*$, is described by the cross section

$$\sigma(HH^* \rightarrow \phi\phi^*) = \frac{1}{4} \frac{\kappa^2}{16\pi s}, \quad (33)$$

neglecting all masses. After the electroweak phase transition, there are three such annihilations at tree-level: $hh, VV, f\bar{f} \rightarrow \varphi\varphi$, where V is a vector gauge boson that could be either the W or Z , and f is any SM fermion. Both VV and $f\bar{f}$ scattering are s -channel processes mediated by the Higgs, consequently $t\bar{t}$ scattering is much larger than any other fermion scattering due

to the dominance of y_t over all other Yukawas. The production of φ from these annihilations is subdominant compared to the three-body processes $h \rightarrow \varphi\varphi$ and $hh \rightarrow \varphi$ when either is kinematically allowed. However, for $m_h/2 \leq m_\varphi \leq 2m_h$ only scattering is allowed, therefore it entirely determines the injection of energy into the ϕ bath.

Higgs scattering

There are seven tree-level diagrams which mediate $hh \rightarrow \varphi\varphi$. The three dominant diagrams are the contact interaction and the two s-channel diagrams, one with a virtual h , the other with a virtual φ . The two t-channel diagrams and two u-channel diagrams (with virtual h or φ) are suppressed by an extra factor of $\kappa \ll 1$ and therefore negligible. The squared matrix element is then

$$|\mathcal{M}(hh \rightarrow \varphi\varphi)|^2 \simeq \frac{\kappa^2(s + 2m_h^2)^2(s + 2m_\varphi^2)^2}{(s - m_h^2)^2(s - m_\varphi^2)^2}, \quad (34)$$

where we dropped terms involving the h and φ widths, since $\Gamma_{h,\varphi} \ll m_{h,\varphi}$ and $s \geq \max\{4m_h^2, 4m_\varphi^2\}$.

The collision term is

$$2 \int \frac{d^3p_\varphi}{(2\pi)^3} E_\varphi \mathcal{C}_\varphi[hh \rightarrow \varphi\varphi] = \frac{m_h^5}{2^{11}\pi^5 x^5} \int_{4x^2}^\infty dr \sqrt{r - 4x_{\varphi T}^2} \sqrt{r - 4x^2} K_1(\sqrt{r}) |\mathcal{M}(hh \rightarrow \varphi\varphi)|^2 \Theta(r - 4x_{\phi T}^2), \quad (35)$$

where $x_{\varphi T} = m_\varphi/T$, taking a Maxwell-Boltzmann (MB) distribution for the Higgs. Using a Bose-Einstein (BE) distribution instead gives a similar result.

Vector boson scattering

Vector-boson scattering is an s -channel processes mediated by the Higgs, with cross-section

$$\sigma(VV \rightarrow \varphi\varphi) = \frac{1}{9} \frac{\kappa^2}{32\pi s} \sqrt{\frac{s - 4m_\varphi^2}{s - 4m_V^2}} \frac{s^2 - 4sm_V^2 + 12m_V^4}{(s - m_h^2)^2}, \quad (36)$$

averaging over polarisations, where we again neglect the Higgs decay width. Then the collision term is

$$2 \int \frac{d^3p_\varphi}{(2\pi)^3} E_\varphi \mathcal{C}_\varphi[VV \rightarrow \varphi\varphi] = \frac{\kappa^2 m_h^5}{2^{11}\pi^5 x^5} \sum_V \int_{4x_V^2}^\infty dr \sqrt{r - 4x_V^2} \sqrt{r - 4x_{\varphi T}^2} \frac{12x_V^4 - 4rx_V^2 + r^2}{(r - x^2)^2} \times K_1(\sqrt{r}) \Theta(r - 4x_{\varphi T}^2), \quad (37)$$

where $x_V = m_V/T$, using a MB distribution for the vector bosons.

Top quark scattering

Like vector-boson scattering, $t\bar{t}$ scattering occurs via an s -channel diagram with a virtual Higgs. The cross-section is

$$\sigma(t\bar{t} \rightarrow \varphi\varphi) = \frac{1}{192\pi s} \frac{\kappa^2 m_t^2 \sqrt{(s - 4m_\varphi^2)(s - 4m_t^2)}}{(s - m_h^2)^2}, \quad (38)$$

averaging over initial spins and colours. The collision term is

$$2 \int \frac{d^3 p_\varphi}{(2\pi)^3} E_\varphi \mathcal{C}_\varphi[t\bar{t} \rightarrow \varphi\varphi] = \frac{6\kappa^2 m_t^2 m_h^3}{2^{10} \pi^5 x^3} \int_{4x_t^2}^\infty dr \frac{\sqrt{r - 4x_{\varphi T}^2} (r - 4x_t^2)^{3/2}}{(r - x^2)^2} K_1(\sqrt{r}) \Theta(r - 4x_{\varphi T}^2), \quad (39)$$

where $x_t = m_t/T$ and $\tilde{\Gamma}_h = \Gamma_h/T$, taking a MB distribution for the top.

The collision terms from Higgs, vector boson and top quark scattering are all approximately the same order of magnitude since $\lambda \sim g_{1,2} \sim y_t$, therefore no process can be ignored. As mentioned above, scatterings involving lighter fermions are suppressed by their small Yukawa couplings, $y_f \ll y_t$, and are therefore negligible.

C. $hh \rightarrow \varphi$ inverse decay

When $m_\varphi > 2m_h$ and $T_\phi < T_{\phi,c}$, the $hh \rightarrow \varphi$ process opens up and in fact dominates the annihilations considered just above because these 4-body processes are relatively suppressed by an additional phase space factor. Since φ production is peaked at around $T \sim m_\varphi$, at which time the Higgs may be relativistic, we take a BE distribution for the Higgs here. Then we obtain the collision term,

$$\begin{aligned} \int \frac{d^3 p_\varphi}{(2\pi)^3} E_\varphi \mathcal{C}_\varphi[hh \rightarrow \varphi] &= \frac{m_h^3 |\mathcal{M}(hh \rightarrow \varphi)|^2}{32\pi^3 x^3} \int_{x_{\varphi T}}^\infty dF_{\varphi T} \frac{F_{\varphi T}}{e^{F_{\varphi T}} - 1} \ln \left[\text{csch} \left(\frac{F_{\varphi T} - y_{\varphi T} \sqrt{1 - \frac{4m_h^2}{m_\varphi^2}}}{4} \right) \right. \\ &\quad \left. \times \sinh \left(\frac{F_{\varphi T} + y_{\varphi T} \sqrt{1 - \frac{4m_h^2}{m_\varphi^2}}}{4} \right) \right], \end{aligned} \quad (40)$$

where here $F_{\varphi T} = E_\varphi/T$ and $y_{\varphi T} = p_\varphi/T$, with the squared matrix element

$$|\mathcal{M}(hh \rightarrow \varphi)|^2 = \kappa^2 v_\phi^2 \left(\frac{2m_h^2 + m_\varphi^2}{m_\varphi^2 - m_h^2} \right)^2. \quad (41)$$

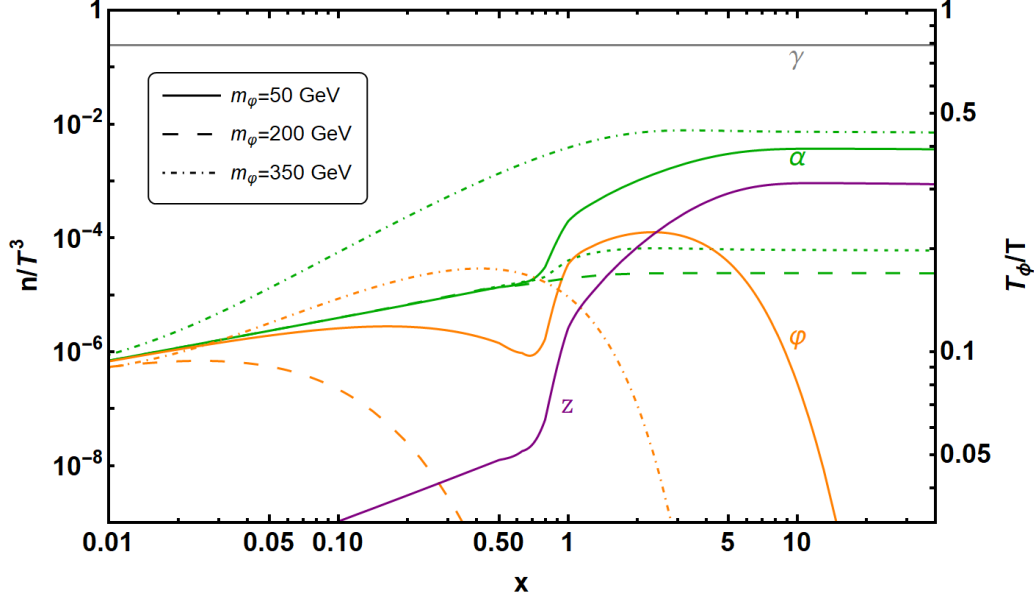


FIG. 3. Number densities of α (green) and ϕ (orange) for different values of $m_\phi = 50(200)[350]$ GeV using solid (dashed) [dotted] lines, with $\lambda_\phi = 0.1$ and $\kappa = 10^{-8}$. We show the evolution of z for $m_\phi = 50$ GeV in purple. For the $m_\phi = 50$ and 350 GeV cases, the ϕ sector remains in equilibrium until production is complete, i.e. until n_α/T^3 reach their final values. For the $m_\phi = 200$ GeV case, equilibration only lasts until $x \simeq 0.4$. The dashed green line shows the true α number density while the dotted green line gives its value had thermalisation persisted.

D. Remarks on the dark sector temperature ratio z

Having computed all the collision terms, we can insert Eqns. (30), (35), (37), (39), and (40) into Eqn. (29) to find z in general. We can make several observations about the form of z . Firstly, since all collision terms are proportional to κ^2 , we have from Eqn. (29) that $z \propto \sqrt{\kappa}$. Moreover, the collision terms are all independent of m_N , therefore so is z . This was already mention in Section III, where we argued that the relic abundance scales as $\Omega_N h^2 \propto \kappa^{3/2} m_N$.

Secondly, the collision terms are positive and approach 0 as x grows much larger than 1. This means that z increases with x , up to shifts in g_* due to entropy dilution of the SM thermal bath as SM fields freeze out. However, at some $m_N \ll T \ll m_h$, the energy injection into the $\phi - N$ bath becomes tiny and consequently z reaches its maximum, after which it decreases slightly due to this entropy dilution.

In Fig. 3 we illustrate the evolution of the number densities of the two new scalars, α (green) and ϕ (orange), for fixed couplings in the scalar potential, $\lambda_\phi = 0.1$ and $\kappa = 10^{-8}$. We represent different scalar masses, $m_\phi = 50(200)[350]$ GeV, by the solid (dashed) [dotted] lines. For

all three masses, the number density of the pNGB α normalised to T^3 approaches a constant value for large x . As α is in thermal equilibrium, its number density is fixed by the temperature ratio z , with $n_\alpha \sim z^3$. Note that n_α , and hence z , is larger for $m_\varphi = 50, 350$ GeV than for the intermediate mass, $m_\varphi = 200$ GeV. This is due to the efficient $h \rightarrow \varphi\varphi$ decay (for $m_\varphi \leq m_h/2$) and $hh \rightarrow \varphi$ inverse decay ($m_\varphi \geq 2m_h$) processes, respectively. All number densities initially increase relative to the photon number density. The α number density freezes in for $x \sim 1 - 5$ and the φ number density is exponentially suppressed when φ becomes non-relativistic at $m_\varphi \simeq T_\phi = zm_h/x$, i.e. at $x \simeq zm_h/m_\varphi$. Note that the exponential suppression when $m_\varphi = 350$ GeV occurs later than when $m_\varphi = 200$ GeV—this is due to the larger temperature ratio z in the former case.

For $m_\varphi = 50$ and 350 GeV, the ϕ sector is in equilibrium throughout the period of its production and therefore the φ and α are well described by thermal number densities. On the other hand, for $m_\varphi = 200$ GeV, the $\varphi\varphi \leftrightarrow \alpha\alpha$ rate drops out of equilibrium around $x \simeq 0.4$ and a non-zero chemical potential develops for $x \gtrsim 0.4$, while kinetic equilibrium is maintained. Consequently, the α number density is approximately a factor of 2.5 smaller than it would be had thermalisation endured throughout its production, as shown by the discrepancy between the dashed green line (the true number density) and the dotted one (number density assuming thermalisation).

Having computed the evolution of T_ϕ , we now investigate the conditions under which dark sector thermalisation occurs.

V. THERMALISATION OF THE ϕ BATH

In this section we consider the thermalisation of the ϕ bath. The assumption of thermalisation was used to compute the sterile neutrino yield analytically, to calculate the temperature evolution of the bath encoded in $z(x)$, and to find N_{eff} and λ_{FS} . This assumption must of course be verified. The strength of ϕ sector interactions is characterised by the quartic coupling, λ_ϕ .

For a process $a + X \leftrightarrow Y$ with X, Y denoting an arbitrary number of particles, the thermally-averaged collision rates which are relevant for kinetic equilibrium of particle species a are defined as

$$\langle \Gamma(aX \leftrightarrow Y) \rangle_a = \frac{1}{n_a} \int \frac{g_a d^3 p_a}{(2\pi)^3} \mathcal{C}_a[aX \leftrightarrow Y], \quad (42)$$

where \mathcal{C}_a denotes the collision term introduced in Eqn. (17). A similar expression applies for the inverse process. For chemical equilibrium, we are concerned with the relaxation rate Γ_{relax} .

For a relativistic particle, it is given by the collision rate, $\Gamma_{\text{coll}} = \langle \Gamma \rangle$, while for a non-relativistic particle it receives a suppression and is given by [44]

$$\Gamma_{\text{relax},a} \simeq (T/m_a) \Gamma_{\text{coll},a}. \quad (43)$$

For $T_\phi > T_{\phi,c}$, the relevant processes for chemical and kinetic equilibration are $\phi\phi \rightarrow \phi\phi\phi\phi^*$ and $\phi\phi \rightarrow \phi\phi$, together with processes where some ϕ are replaced by the antiparticle ϕ^* . We use the results in [31, 45] to estimate thermalisation for the intermediate ranges above the critical temperature. More importantly, for $T_\phi < T_{\phi,c}$ the relevant processes are $\varphi \leftrightarrow \alpha\alpha$, $\varphi\varphi \leftrightarrow \alpha\alpha$, and $\alpha\varphi \rightarrow \alpha\varphi$, whose rates are

$$\Gamma(\varphi \rightarrow \alpha\alpha) = \frac{\lambda_\phi m_\varphi}{16\pi} \quad (44)$$

$$\sigma(\varphi\varphi \rightarrow \alpha\alpha) = \frac{\lambda_\phi^2}{4\pi\sqrt{s(s-4m_\varphi^2)}} \quad (45)$$

$$\times \left[1 + \frac{(2m_\varphi^2 + s)^2}{2(m_\varphi^2 - s)^2} + \frac{3m_\varphi^4 + m_\varphi^2 s - s^2}{s^2 - 3m_\varphi^2 s + 2m_\varphi^4} \frac{4m_\varphi^2}{\sqrt{s(s-4m_\varphi^2)}} \text{arctanh} \left(\frac{2\sqrt{s(s-4m_\varphi^2)}}{2s - 4m_\varphi^2} \right) \right]$$

$$\sigma(\alpha\alpha \rightarrow \varphi\varphi) = \sigma(\varphi\varphi \rightarrow \alpha\alpha) \left(1 - \frac{4m_\varphi^2}{s} \right) \quad (46)$$

$$\sigma(\alpha\varphi \rightarrow \alpha\varphi) \simeq \frac{\lambda_\phi^2}{4\pi m_\varphi^2} \left(\frac{s^6 + 4m_\varphi^2 s^5 + 29m_\varphi^4 s^4 + 4m_\varphi^6 s^3 + 29m_\varphi^8 s^2 + 4m_\varphi^{10} s + m_\varphi^{12}}{3m_\varphi^4 s^2 (s^2 - m_\varphi^2 s + m_\varphi^4)} - \frac{6(s + m_\varphi^2)^2}{(s - m_\varphi^2)^2} \ln \frac{s^2 - m_\varphi^2 s + m_\varphi^4}{m_\varphi^2 s} \right). \quad (47)$$

We neglected the u -channel contribution in the cross section for $\alpha\varphi \rightarrow \alpha\varphi$, where the self-energy plays an important role. These issues are discussed in App. A, where we give the expressions for this self-energy, and App. B, where we explain that this contribution is generally negligible but is very computationally taxing. For $\varphi \rightarrow \alpha\alpha$ and $\varphi\varphi \rightarrow \alpha\alpha$, the relaxation rate is equal to the collision rate $\Gamma_{\text{relax}} = \Gamma_{\text{coll}}$, while for processes with the scalar φ in the final state, it is given by $\Gamma_{\text{relax}} \approx \Gamma_{\text{coll}}/x_\varphi$, where

$$x_\varphi \equiv \frac{m_\varphi}{T_\phi}. \quad (48)$$

When all relevant interaction rates are faster than the Hubble rate, thermalisation is guaranteed. Hence, the conditions for thermalisation are

$$\langle \Gamma(\varphi \leftrightarrow \alpha\alpha) \rangle_\alpha > H \quad (49)$$

$$\langle \Gamma(\varphi\varphi \leftrightarrow \alpha\alpha) \rangle_\alpha > H \quad (50)$$

$$x_\varphi^{-1} \langle \Gamma(\alpha\varphi \rightarrow \alpha\varphi) \rangle_\varphi > H, \quad (51)$$

where the conditions in the first two lines ensure kinetic and chemical equilibrium for α and chemical equilibrium for φ . The corresponding interaction rates in the Boltzmann equations of φ are automatically satisfied in this case. The last condition ensures kinetic equilibrium of φ . We will demonstrate the thermalisation in two stages. First we find when a non-thermal distribution described by a delta function thermalises quickly enough, then we calculate when a thermal distribution of φ and α particles remains in thermal equilibrium.

Note that the pNGB plays an important role in thermalising the dark sector, in fact takes part in all relevant processes. This is the main difference to the thermalisation of the real scalar field. In [31] the authors find that for the heavy scalar, analogous to our φ , thermalisation can be achieved via $\varphi\varphi \rightarrow \varphi\varphi\varphi\varphi$ but only for larger couplings, e.g. for $m_\varphi \gtrsim 100$ GeV they require $\kappa \gtrsim 10^{-9}$ and $\lambda_\phi \gtrsim 0.1$.

A. Initial ϕ thermalisation

The thermal averaging depends on the distribution functions of the particles involved in the given interaction. If they are already in equilibrium, we can take a MB, BE or FD distribution as appropriate. If the particles are not in equilibrium, however, their distribution functions can in general only be found by numerically solving a Boltzmann equation. To avoid this complication, we will assume below that at early times the φ , α , and N have delta function distributions. This is motivated by the instantaneous decay approximation. For a homogeneous distribution of non-relativistic Higgs bosons, the distribution of φ in the instantaneous decay approximation is homogeneous and isotropic with a definite energy, since h is a scalar which dominantly decays at rest. After averaging over the homogeneous and isotropic initial states, the resulting distributions for inverse decays and $2 \rightarrow 2$ scattering processes are also homogeneous and isotropic. In order to obtain semi-analytic estimates, and to model an extremely non-thermal distribution, we assume that the φ distributions for inverse decay and $2 \rightarrow 2$ scattering processes have a definite energy which is determined by the centre of mass energy of the collisions. This neglects the velocity dispersion of the initial state particles, which leads to a broadening of the φ distribution. A detailed discussion requires to solve the Boltzmann equations numerically and is beyond the scope of this study. Consider non-thermal distributions described by the delta functions,

$$f_\alpha(p_\alpha) = C_\alpha \delta(p_\alpha - X_\alpha) \qquad f_\varphi(E_\varphi) = C_\varphi \delta(E_\varphi - X_\varphi), \qquad (52)$$

with $p_\alpha \equiv |\vec{p}_\alpha|$. The number densities are

$$n_\alpha = \int \frac{d^3 p_\alpha}{(2\pi)^3} f_\alpha = \frac{C_\alpha X_\alpha^2}{2\pi^2} \quad n_\varphi = \int \frac{d^3 p_\varphi}{(2\pi)^3} f_\varphi = \frac{C_\varphi X_\varphi \sqrt{X_\varphi^2 - m_\varphi^2}}{2\pi^2}, \quad (53)$$

and thus $C_\alpha = 2\pi^2 n_\alpha / X_\alpha^2$ and $C_\varphi = 2\pi^2 n_\varphi / (X_\varphi^2 \sqrt{1 - m_\varphi^2 / X_\varphi^2})$. With the φ and α distribution functions thus defined, the thermally-averaged interaction rates are

$$\langle \Gamma(\varphi \rightarrow \alpha\alpha) \rangle_\alpha = \frac{C_\varphi m_\varphi X_\varphi}{\pi^2 n_\alpha} \Gamma(\varphi \rightarrow \alpha\alpha) \sqrt{1 - \frac{m_\varphi^2}{X_\varphi^2}} \quad (54)$$

$$\langle \Gamma(\alpha\alpha \rightarrow \varphi) \rangle_\alpha = \frac{C_\alpha^2 m_\varphi}{2\pi^2 n_\alpha} \Gamma(\varphi \rightarrow \alpha\alpha) \theta(2X_\alpha - m_\varphi) \quad (55)$$

$$\langle \Gamma(\varphi\varphi \rightarrow \alpha\alpha) \rangle_\alpha = \frac{C_\varphi^2 m_\varphi^4}{4\pi^4 n_\alpha} \int_1^{\frac{X_\varphi^2}{m_\varphi^2}} d\xi \sigma(s = 4m_\varphi^2 \xi) \sqrt{\xi(\xi - 1)} \quad (56)$$

$$\langle \Gamma(\alpha\alpha \rightarrow \varphi\varphi) \rangle_\alpha = \frac{C_\alpha^2 m_\varphi^4}{4\pi^4 n_\alpha} \int_1^{\frac{X_\alpha^2}{m_\varphi^2}} d\xi \sigma(s = 4m_\varphi^2 \xi) (\xi - 1) \quad (57)$$

$$\langle \Gamma(\alpha\varphi \rightarrow \alpha\varphi) \rangle_\varphi = \frac{C_\alpha C_\varphi m_\varphi^4}{32\pi^4 n_\varphi} \int_1^{\frac{(X_\varphi + X_\alpha)^2}{m_\varphi^2}} d\xi \sigma(s = m_\varphi^2 \xi) (\xi - 1) \Theta \left(X_\varphi + X_\alpha - \frac{4X_\alpha^2 \xi + m_\varphi^2 (\xi - 1)^2}{4X_\alpha (\xi - 1)} \right). \quad (58)$$

Now, as an approximation, let us take $X_\varphi = \langle E_h \rangle / 2$ when $m_\varphi < m_h / 2$, $X_\varphi = \langle E_h \rangle$ when $2m_h \geq m_\varphi \geq m_h / 2$, and $X_\varphi = 2\langle E_h \rangle$ when $m_\varphi > m_h / 2$, where $\langle E_h \rangle = \rho_h / n_h$. We make this m_φ -dependent approximation since, as discussed above, φ production is dominated by $h \rightarrow \varphi\varphi$ in the smallest mass region, by $hh, t\bar{t}$ and VV scattering to $\varphi\varphi$ in the intermediate regime, and by $hh \rightarrow \varphi$ in the heavy mass region. Then, since the φ particles rapidly decay via $\varphi \rightarrow \alpha\alpha$, we take as the initial condition that the α energy is half the φ energy, i.e. $X_\alpha = X_\varphi / 2$. We note for $m_\varphi > m_h$ that at sufficiently late times $X_\varphi < m_\varphi$, which is unphysical. Therefore, we impose that equilibration must occur while $X_\varphi > m_\varphi$.

We compute the φ number density by summing over the processes which produce it, outlined in Sec. IV, then assume that the ϕ sector interactions are sufficiently strong that the φ and α number densities are approximately equal. Thus, given $n_{\varphi,\alpha}$ and $X_{\varphi,\alpha}$, we can find $C_{\varphi,\alpha}$ from Eqn. (53). It enables a calculation of the various thermalisation rates listed above, thereby allowing us to find the region of parameter space in which the ϕ sector equilibrates, given these assumptions.

B. Continued ϕ thermalisation

If the ϕ sector enters into equilibrium, we want to find for how long it maintains it. For this step, we can evaluate the collision rates given thermal distributions of φ and α . As the interaction rates with BE distributions are strictly larger than the ones with MB distributions, $f_{BE} > f_{MB}$, we will make a conservative estimate and approximate all distributions by MB ones, as well as neglecting the $(1 + f)$ Bose-enhancement factors. Given this, we find

$$\langle \Gamma(\varphi \leftrightarrow \alpha\alpha) \rangle_\alpha = \frac{m_\varphi^3 K_1(x_\varphi)}{2\pi^2 x_\varphi n_\alpha} \Gamma(\varphi \rightarrow \alpha\alpha) \quad (59)$$

$$\langle \Gamma(\varphi\varphi \leftrightarrow \alpha\alpha) \rangle_\alpha = \frac{m_\varphi^6}{2\pi^4 x_\varphi n_\alpha} \int_1^\infty d\xi \sqrt{\xi}(\xi - 1) K_1(2x_\varphi \sqrt{\xi}) \sigma(s = 4m_\varphi^2 \xi) \quad (60)$$

$$\langle \Gamma(\alpha\varphi \rightarrow \alpha\varphi) \rangle_\varphi = \frac{m_\varphi^6}{32\pi^4 x_\varphi n_\varphi} \int_1^\infty d\xi \frac{(\xi - 1)^2}{\sqrt{\xi}} \sigma(s = m_\varphi^2 \xi) K_1(x_\varphi \sqrt{\xi}). \quad (61)$$

Inserting these rates into Eqns. (49), (50) and (51) tells us for how long the ϕ sector remains in equilibrium. Note that $\langle \Gamma(\varphi \rightarrow \alpha\alpha) \rangle_\varphi = \langle \Gamma(\alpha\alpha \rightarrow \varphi) \rangle_\alpha$ and $\langle \Gamma(\varphi\varphi \rightarrow \alpha\alpha) \rangle_\varphi = \langle \Gamma(\alpha\alpha \rightarrow \varphi\varphi) \rangle_\alpha$ by detailed balance.

C. Discussion

We illustrate the rates which are relevant for thermalisation for one particular benchmark point with $\lambda_\phi = 0.1$, $\kappa = 10^{-8}$ and $m_\varphi = 50$ GeV in Fig. 4. The figure displays the relaxation rates for $T_\phi < T_{\phi,c}$ for the different processes, normalised to the Hubble rate, as a function of x . The case for $T_\phi > T_{\phi,c}$ has been discussed in [45] and the results presented in their Fig. 2. Taking into account the differences in the model (real vs complex scalar), we conclude that for $m_\phi = 50$ GeV thermalisation is reached for $\lambda_\phi \gtrsim 10^{-3}$. This is consistent with Fig. 4, which shows that thermalisation of the ϕ sector is easily achieved at early times.

In the following, we entirely focus on the rates for $T_\phi < T_{\phi,c}$ which determine the thermalisation of the ϕ sector at late times. The rates for initial thermalisation are shown as dashed lines and for continued thermalisation as solid ones. When all the dashed lines go above $\Gamma/H = 1$, there is initial equilibration: from this time on, the ϕ sector particles are well approximated by equilibrium distributions and the solid lines become the relevant ones. For $x < 0.78$, electroweak symmetry is intact and the production of the ϕ sector particles only occurs via $HH^* \rightarrow \phi\phi^*$. Since the relaxation rates, Γ , are larger than the Hubble rate for $x < 0.78$ in Fig. 4, the dark sector quickly thermalises with a temperature $T_\phi = zT$. As $z \lesssim 0.1$, the scalar φ becomes non-relativistic (cf. Fig. 3) and the interaction rates become Boltzmann suppressed,

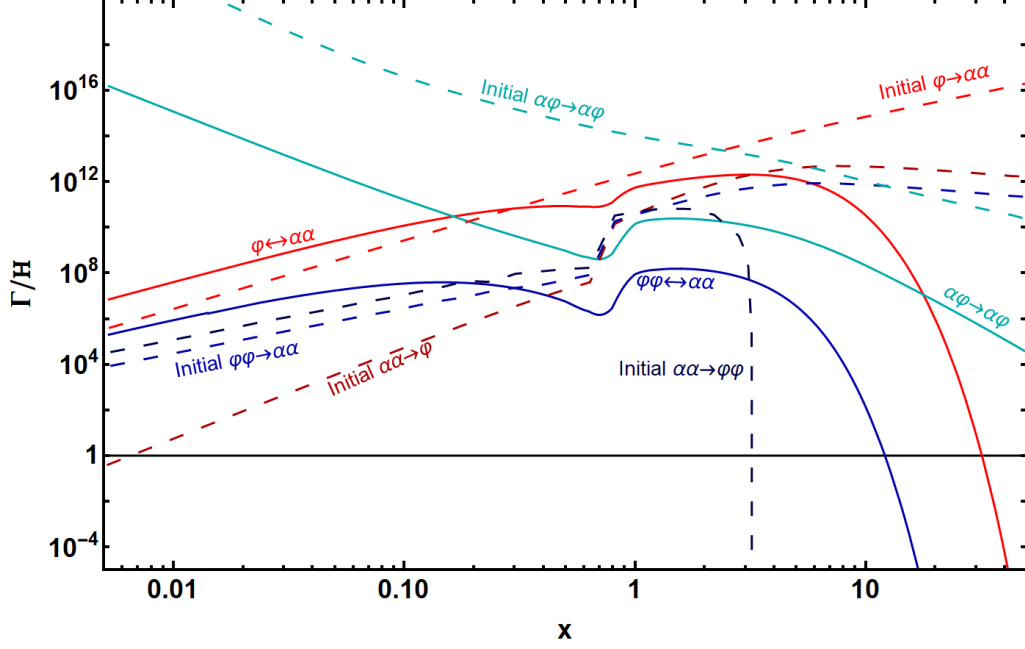


FIG. 4. Relaxation rates in the ϕ sector normalised to the Hubble rate as a function of x for $\lambda_\phi = 0.1$, $\kappa = 10^{-8}$, $m_\phi = 50$ GeV. See the solid lines in Fig. 2 for the evolution of the different abundances.

which is apparent from the drop in the continued relaxation rates around $x \lesssim 0.78$. After the electroweak phase transition at $x \geq 0.78$, Higgs decays become possible and indeed dominate the energy transfer to the dark sector, ultimately leading to increased relaxation rates since T_ϕ/T grows.

The fast drop in the continued relaxation rates $\phi \leftrightarrow \alpha\alpha$ and $\phi\phi \leftrightarrow \alpha\alpha$ originates from the Bessel function K_1 in the interaction rates, which leads to an exponential suppression for large x_ϕ . It becomes exponentially difficult to produce ϕ particles at lower temperatures, and thus their abundance is suppressed. The continued rate for $\alpha\phi \rightarrow \alpha\phi$ falls off slower because there is a large number of pNGBs α relative to the number of scalars ϕ , which are able to transfer energy to the ϕ and keep them in kinetic equilibrium. Initial rates do not suffer Boltzmann suppression, since they do not assume that the ϕ sector equilibrates. The ϕ and α number density is given by the number of Higgs decays/scatterings, which eventually plateaus. While the $\phi \rightarrow \alpha\alpha$ initial rate keeps growing, the others decrease (and the $\alpha\alpha \rightarrow \phi\phi$ rate vanishes) at large x because the particles lose energy.

In our numerical study, we consider thermal equilibrium to be reached if there is a period of time when the conditions for initial thermalisation hold, directly followed by a period of time when the conditions for continued thermalisation hold, until at least 80% of the ϕ have been produced. This is satisfied above the solid contours in Fig. 5. By contrast, the dotted contours

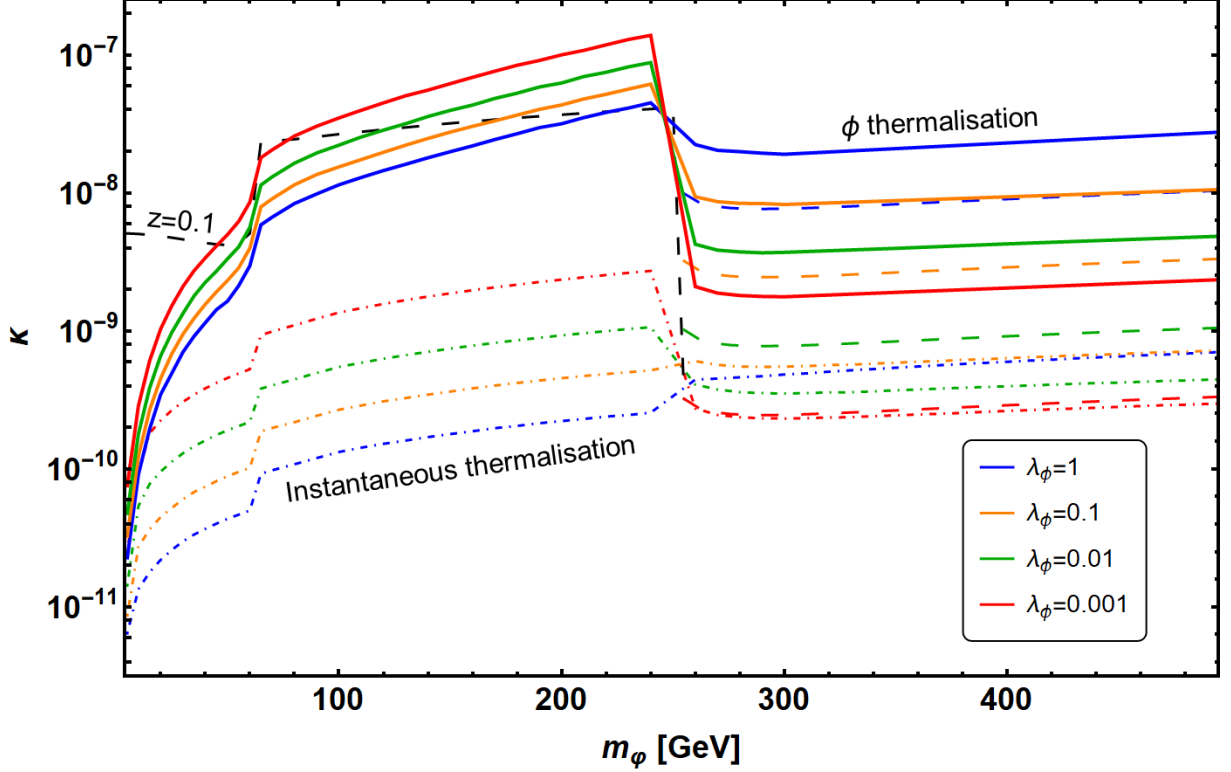


FIG. 5. Portal coupling κ required for ϕ sector thermalisation until at least 80% of the ϕ have been produced (solid contours), assuming instantaneous thermalisation is possible (i.e. one instant of all relaxation rates larger being larger than the Hubble rate is sufficient, dotted contours), and for $z = 0.1$ at late times (dashed contours). For $m_\phi \leq 2m_h$, the value of z is λ_ϕ -independent, however for $m_\phi > 2m_h$ it depends on λ_ϕ via the $hh \rightarrow \phi$ process. The observed dark matter abundance requires $z \simeq 0.1$, therefore above the dashed contours the sterile neutrino abundance would be too large.

indicate the values of κ required for instantaneous thermalisation, i.e. that there is at least one time during ϕ production that initial thermalisation and then continued thermalisation was achieved. It is notable that this is a significantly weaker condition. Fig. 5 shows that for instantaneous thermalisation, values of κ that are smaller by 1-2 orders of magnitude are allowed compared to those which enable sustained thermalisation during the period of dominant ϕ production. The dashed contours denote where $z = 0.1$ is reached at late times, which indicates the relevant region of parameter space where the observed dark matter abundance is obtained. For $m_\phi \leq 2m_h$, this is independent of λ_ϕ and is represented by a black line, while for $m_\phi > 2m_h$, it depends on λ_ϕ through the process $hh \rightarrow \phi$, as can be seen from Eqn. (41).

For light ϕ scalars with $m_\phi < m_h/2$ the ϕ sector is efficiently heated via Higgs decays to a pair of ϕ scalars and thus thermalisation is reached even for small portal couplings $\kappa \sim 10^{-11} - 10^{-10}$. When $h \rightarrow \phi\phi$ becomes unavailable, the portal coupling κ has to be substantially larger to heat

the ϕ sector and thermalisation is only achieved for larger $\kappa \sim 10^{-8}$. For large φ masses, $m_\varphi > 2m_h$, although inverse Higgs decays $hh \rightarrow \varphi$ efficiently heat up the ϕ sector, the production of dark sector particles generally extends beyond the time when the dark sector drops out of thermal equilibrium and thus the resulting ϕ sector distribution does not follow a Bose-Einstein distribution. We find that for smaller λ_ϕ , smaller values of κ lead to thermalisation because the interaction rate of $hh \rightarrow \varphi$ scales like λ_ϕ^{-1} , again see Eqn. (41). This implies that T_ϕ is larger for smaller values of λ_ϕ , which counteracts the increase of the relaxation rates for increasing λ_ϕ . Overall, we observe that thermalisation generally requires $\kappa \gtrsim 10^{-9} - 10^{-8}$.

While thermalisation is achieved above the solid contours, the observed dark matter abundance is obtained close to the dashed contours. The analysis demonstrates that the dark matter will not follow a thermal distribution for $m_\varphi > 2m_h$ irrespective of the value of λ_ϕ . For $m_\varphi < m_h/2$, where Higgs decay $h \rightarrow \varphi\varphi$ is allowed, the value of κ required to achieve $z = 0.1$ is large enough to equilibrate the ϕ sector even for $\lambda_\phi \simeq 10^{-3}$. For $m_h/2 < m_\varphi < 2m_h$, the values of κ to achieve $z = 0.1$ are close to the thermalisation boundary and thus whether thermalisation is achieved or not depends on the quartic coupling λ_ϕ .

VI. THERMALISATION OF STERILE NEUTRINOS

Having outlined above the conditions for the ϕ sector to thermalise, we now turn to the conditions for sterile neutrino equilibration with the ϕ bath. The $\phi - N$ interactions depend on the Yukawa coupling, f , cf. Eqn. (14). Since we assume that $f = \sqrt{2}m_N/v_\phi \ll 1$ while λ_ϕ can be $\mathcal{O}(1)$, the timescales of thermalisation are different. We can therefore consider it to be a two-step process in which the sterile neutrinos only thermalise after the ϕ sector has already reached equilibrium. Thus, it is safe to entirely neglect the range of $T_\phi > T_{\phi,c}$ and to focus on temperatures T_ϕ below the critical dark sector temperature.

If the rates of $\varphi \leftrightarrow NN$, $\alpha\alpha \leftrightarrow NN$ and $\alpha N \rightarrow \alpha N$ are larger than the Hubble rate, then the sterile neutrinos thermalise and join the ϕ bath. In fact, it is sufficient for only one of $\varphi \leftrightarrow NN$ or $\alpha\alpha \leftrightarrow NN$ to be in equilibrium, as long as the ϕ sector remains in thermal equilibrium. The key conditions for thermalisation are therefore either of

$$\langle \Gamma(\varphi \leftrightarrow NN) \rangle_N > H, \quad \langle \Gamma(\alpha\alpha \leftrightarrow NN) \rangle_N > H. \quad (62)$$

The process $\alpha N \rightarrow \alpha N$ also ensures kinetic equilibrium of N for $\langle \Gamma(\alpha N \rightarrow \alpha N) \rangle_N > H$, however $\varphi \leftrightarrow NN$ and $\alpha\alpha \leftrightarrow NN$ are sufficient to achieve both chemical and kinetic equilibrium. Note that in principle a second possibility is that N enters its own thermal bath via $NN \rightarrow NN$

scatterings, even if it does not equilibrate with the ϕ sector. The relevant decay widths and cross sections are

$$\Gamma(\varphi \rightarrow NN) = \frac{\lambda_\phi m_N^2}{8\pi m_\varphi} \quad (63)$$

$$\begin{aligned} \sigma(NN \rightarrow \alpha\alpha) \simeq \lim_{\epsilon \rightarrow 0} \frac{\lambda_\phi^2 m_N^2}{16\pi m_\varphi^2 s} & \left[\frac{m_\varphi^2 s (m_\varphi^2 + \Gamma_\varphi^2 - s)^2}{((s - m_\varphi^2)^2 + m_\varphi^2 \Gamma_\varphi^2)^2} \right. \\ & \left. + \frac{s^3 \Gamma_\varphi^2}{((s - m_\varphi^2)^2 + m_\varphi^2 \Gamma_\varphi^2)^2} \left(1 - 2\epsilon^3 \left[\frac{(s - m_\varphi^2)^2 + m_\varphi^2 \Gamma_\varphi^2}{(s - m_\varphi^2)^2 + \epsilon^2 m_\varphi^2 \Gamma_\varphi^2} \right]^2 \right) \right] \end{aligned} \quad (64)$$

$$\sigma(\alpha\alpha \rightarrow NN) = 4\sigma(NN \rightarrow \alpha\alpha) \left(1 - \frac{4m_N^2}{s} \right) \quad (65)$$

$$\sigma(\alpha N \rightarrow \alpha N) \simeq \frac{\lambda_\phi^2 m_N^2}{4\pi s^2} \left[\ln \left(1 + \frac{s}{m_\varphi^2} \right) - \frac{s}{m_\varphi^2 + s} \right] \quad (66)$$

$$\begin{aligned} \sigma(NN \rightarrow NN) \simeq \lim_{\epsilon \rightarrow 0} \frac{\lambda_\phi^2 m_N^4}{16\pi s m_\varphi^2} & \left[\frac{3m_\varphi^4 - 3m_\varphi^2 s + 2s^2 + \Gamma_\varphi^2 (s + 3m_\varphi^2)}{((s - m_\varphi^2)^2 + m_\varphi^2 \Gamma_\varphi^2)(s + m_\varphi^2)} \right. \\ & + \frac{4m_\varphi^2 m_\varphi^4 + m_\varphi^2 s - 2s^2 + \Gamma_\varphi^2 (s + m_\varphi^2)}{s ((s - m_\varphi^2)^2 + m_\varphi^2 \Gamma_\varphi^2)(s + 2m_\varphi^2)} \ln \left(1 + \frac{s}{m_\varphi^2} \right) \\ & \left. - \frac{2s^2 \Gamma_\varphi^2 \epsilon^3}{((s - m_\varphi^2)^2 + \epsilon^2 m_\varphi^2 \Gamma_\varphi^2)^2} \right]. \end{aligned} \quad (67)$$

For each, we go to leading order in m_N , which is justified for $s \gg m_N^2$. For $s \ll m_\varphi^2$, the scattering cross section for $NN \rightarrow NN$ can be approximated by

$$\sigma(NN \rightarrow NN) \simeq \frac{5\lambda_\phi^2}{16\pi s} \frac{m_N^4}{m_\varphi^4}. \quad (68)$$

The processes $NN \leftrightarrow \alpha\alpha$ and $NN \leftrightarrow NN$ both involve an s -channel diagram with a virtual φ , and therefore we need to perform real intermediate state subtraction. It is convenient to use the representation of the delta function,

$$\delta(s - m_\varphi^2) = \frac{2}{\pi} \lim_{\epsilon \rightarrow 0} \frac{m_\varphi^3 \Gamma_\varphi^3 \epsilon^3}{((s - m_\varphi^2)^2 + \epsilon^2 m_\varphi^2 \Gamma_\varphi^2)^2}, \quad (69)$$

see Appendix A of [46]. This is shown in Eqns. (64) and (67). For numerical evaluations it suffices to enforce that $\epsilon \ll \Gamma_\varphi/m_\varphi$. We neglect the t - and u -channel diagrams with a virtual N in the calculation, because they are suppressed by an additional factor of f compared to the contact interaction and the s -channel contribution.

For $\alpha N \rightarrow \alpha N$, there are four tree-level diagrams: a contact interaction via the $\alpha^2 N^2$ term in Eqn. (14), an s -channel diagram with a virtual N , a u -channel diagram with a virtual N , and a t -channel diagram with a virtual φ . However, we can neglect the s - and u -channel diagrams

in the calculation because they are suppressed by an additional factor of f compared to the other two diagrams.

As in our study of the ϕ equilibration, we consider thermalisation in two stages. Firstly, in order to determine under what conditions the sterile neutrinos thermalise in the first place, we will assume that they initially have a delta function distribution and find whether they enter into equilibrium. Secondly, assuming that equilibration is achieved, we compute the thermally-averaged rates to find for how long they remain in equilibrium.

A. Initial sterile neutrino thermalisation

Consider the initial conditions that sterile neutrinos have a delta function distribution while the ϕ sector has already equilibrated. The rates $\langle \Gamma(\varphi \rightarrow NN) \rangle_\varphi$ and $\langle \Gamma(\alpha\alpha \rightarrow NN) \rangle_\alpha$ are insensitive to the N distribution, up to negligible Pauli-blocking $(1 - f_N)$ factors in the thermal averaging, therefore we postpone discussion of those to the following subsection. Here we address the processes $NN \rightarrow \varphi$, $NN \rightarrow \alpha\alpha$, $\alpha N \rightarrow \alpha N$ and $NN \rightarrow NN$.

As for the ϕ sector, we describe the initial sterile neutrino distribution by

$$f_N = C_N \delta(E_N - X_N). \quad (70)$$

The N may be produced either by $\varphi \rightarrow NN$ or by $\alpha\alpha \rightarrow NN$. Since $\alpha\alpha \rightarrow NN$ dominates at the earliest times, let us take $X_N = \langle p_\alpha \rangle \simeq 2.7T_\phi$. An estimate for the N number density is $n_N \sim n_\varphi \langle \Gamma(\varphi \rightarrow NN) \rangle_\varphi / H + n_\alpha \langle \Gamma(\alpha\alpha \rightarrow NN) \rangle_\alpha / H$. The number density from the distribution function is

$$n_N = \frac{C_N X_N^2}{2\pi^2} = 0.37 C_N T_\phi^2, \quad (71)$$

neglecting $m_N \ll T_\phi$. We compute $C_N(x_\varphi)$ numerically by equating this to the estimate for n_N from φ decay and α scattering. The thermally averaged rates in the limit $m_N \ll T_\phi$ are

$$\langle \Gamma(NN \rightarrow \varphi) \rangle_N \simeq \frac{2C_N^2 m_\varphi \Gamma(\varphi \rightarrow NN)}{\pi^2 n_N} \quad (72)$$

$$\langle \Gamma(NN \rightarrow \alpha\alpha) \rangle_N \simeq \frac{C_N^2 m_\varphi^4}{16\pi^4 x_\varphi^4 n_N} \int_0^{4\chi_N^2} dr \sigma(s = T_\phi^2 r) r \quad (73)$$

$$\langle \Gamma(\alpha N \rightarrow \alpha N) \rangle_N \simeq \frac{C_N m_\varphi^5}{16\pi^4 x_\varphi^5 n_N} \int_0^\infty dr \sigma(s = T_\phi^2 r) r \left(\frac{r}{4\chi_N} - \ln(e^{r/4\chi_N} - 1) \right) \quad (74)$$

$$\langle \Gamma(NN \rightarrow NN) \rangle_N \simeq \frac{C_N^2 m_\varphi^4}{16\pi^4 x_\varphi^4 n_N} \int_0^{4\chi_N^2} dr \sigma(s = T_\phi^2 r) r, \quad (75)$$

neglecting Bose-enhancement and Pauli-blocking factors, with $\chi_N \equiv X_N/T_\phi$ and $r \equiv s/T_\phi^2$.

B. Continued sterile neutrino thermalisation

The thermally averaged rates when φ , α and N have MB, BE and FD distributions, respectively, are

$$\langle \Gamma(\varphi \leftrightarrow NN) \rangle_N \simeq \frac{\Gamma(\varphi \rightarrow NN) m_\varphi^3}{4\pi^2 x_\varphi^2 n_N} \int_{x_\varphi}^\infty \frac{dF_\varphi}{e^{F_\varphi} + 1} \ln \left[\frac{\cosh \left(\frac{F_\varphi + \sqrt{F_\varphi^2 - x_\varphi^2}}{4} \right)}{\cosh \left(\frac{F_\varphi - \sqrt{F_\varphi^2 - x_\varphi^2}}{4} \right)} \right] \quad (76)$$

$$\langle \Gamma(NN \rightarrow \alpha\alpha) \rangle_N \simeq \frac{m_\varphi^6}{8\pi^4 x_\varphi^6 n_N} \int_0^\infty dr \int_{\sqrt{r}}^\infty dF_+ \frac{\sigma(s = T_\phi^2 r) r}{e^{F_+} - 1} \ln \left[\frac{\cosh \left(\frac{F_+}{4} \left[1 + \sqrt{1 - \frac{r}{F_+^2}} \right] \right)}{\cosh \left(\frac{F_+}{4} \left[1 - \sqrt{1 - \frac{r}{F_+^2}} \right] \right)} \right] \quad (77)$$

$$\langle \Gamma(\alpha N \rightarrow \alpha N) \rangle_N \simeq \frac{m_\varphi^6}{16\pi^4 x_\varphi^6 n_N} \int_0^\infty dr \int_{\sqrt{r}}^\infty dF_+ \frac{\sigma(s = T_\phi^2 r) r}{e^{F_+} + 1} \ln \left[\frac{\sinh \left(\frac{F_+ + \sqrt{F_+^2 - r}}{2} \right)}{\sinh \left(\frac{F_+ - \sqrt{F_+^2 - r}}{2} \right)} \right] \quad (78)$$

$$\langle \Gamma(NN \rightarrow NN) \rangle_N \simeq \frac{m_\varphi^6}{32\pi^4 x_\varphi^6 n_N} \int_0^\infty dr \int_{\sqrt{r}}^\infty dF_+ \frac{\sigma(s = T_\phi^2 r) r}{e^{F_+} - 1} \ln \left[\frac{\cosh \left(\frac{F_+}{4} \left[1 + \sqrt{1 - \frac{r}{F_+^2}} \right] \right)}{\cosh \left(\frac{F_+}{4} \left[1 - \sqrt{1 - \frac{r}{F_+^2}} \right] \right)} \right], \quad (79)$$

again to leading order in m_N . To be conservative, we neglected the $(1 + f_{\varphi,\alpha})$ Bose-enhancement factors in the rates, and for the Pauli-blocking terms in $\alpha N \rightarrow \alpha N$ and $NN \rightarrow NN$ we used the property that $(1 - f_N) \geq 1/2$. We do not separately impose the condition $\langle \Gamma(\alpha\alpha \rightarrow NN) \rangle_N > H$, since it does not pose any new constraint for $4m_N^2 \ll T_\phi^2$. The interaction rate $NN \rightarrow NN$ turns out to be tiny, because the cross section is proportional to m_N^4 and thus very suppressed. We numerically verified that the rate does not reach equilibrium even for the largest sterile neutrino mass and smallest scalar mass that we consider in the analysis, $m_N = 100$ keV and $m_\varphi = 1$ GeV. Consequently, we neglect it in the following discussion. Combining the above with Eqns. (72), (73), and (74), we can find for how long thermalised sterile neutrinos remain in equilibrium.

C. Discussion

In Fig. 6 we illustrate the relaxation rates relative to the Hubble rate as a function of x . The continued $\varphi \leftrightarrow NN$ relaxation rate increases with x until the φ abundance becomes Boltzmann

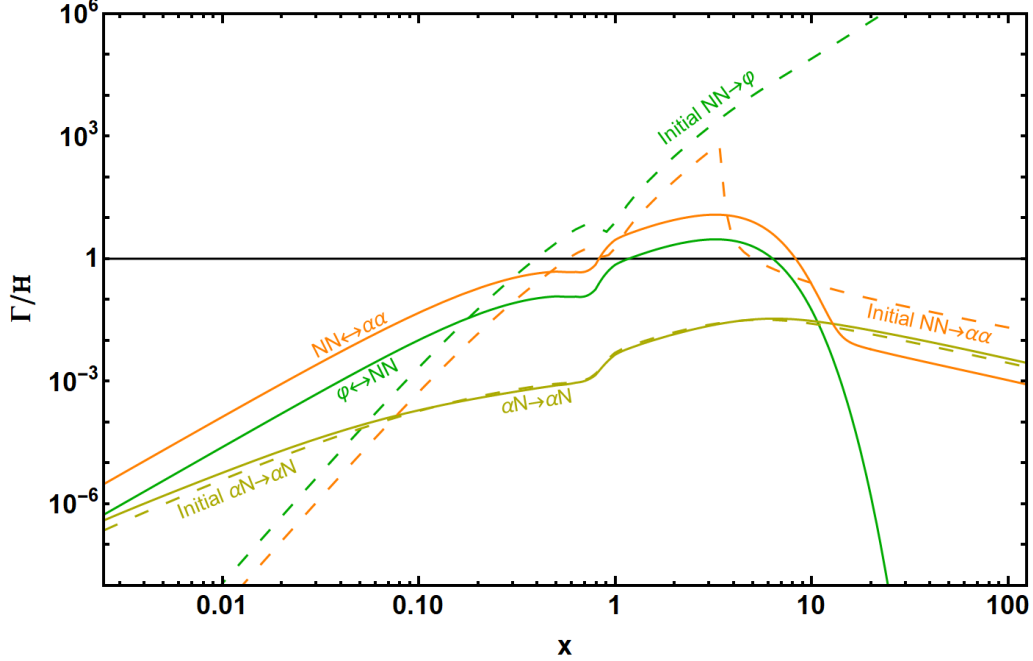


FIG. 6. Relaxation rates of the sterile neutrinos for $\lambda_\phi = 0.1$, $\kappa = 10^{-8}$, $m_\phi = 50$ GeV and $m_N = 80$ keV.

suppressed at $x \gtrsim zm_h/m_\phi$. The continued $\alpha\alpha \leftrightarrow NN$ rates follow a similar trend, but do not show the exponential drop off for large x because they scale as $\Gamma \sim T_\phi^3/m_\phi^2$, as is expected for an effective dimension-5 interaction, see Eqn. (14). The slight drop and subsequent increase in the rates around $x \sim 0.78$ originates from the electroweak phase transition: the scalar ϕ briefly becomes non-relativistic with $T_\phi < m_\phi$, but the increased energy injection from Higgs decays increases the temperature and consequently the rates, cf. the thermalisation of the ϕ sector. The drop in the initial $NN \rightarrow \alpha\alpha$ relaxation rate occurs due to the behaviour of the resonance at $x_\phi = 2X_N$. The resonance region provides the largest contribution for small x , but becomes inaccessible for large x .

The abundance and average energy of the N in the initial thermalisation regime are computed from decays and annihilations of the ϕ and α . At late times, these are suppressed, as indeed we see in Fig. 6. From then on, the N number density and average energy simply scale with the expansion, just like a thermal distribution of relativistic particles. Thus, for large x the initial relaxation rate shows the same scaling as the continued relaxation rate. Finally, both the continued and the initial relaxation rates for the $\alpha N \rightarrow \alpha N$ scattering show the same behaviour which is expected, because we assumed that α is in thermal equilibrium. Following Fig. 4, the ϕ sector remains in chemical equilibrium until $x \sim 12$ and in kinetic equilibrium for

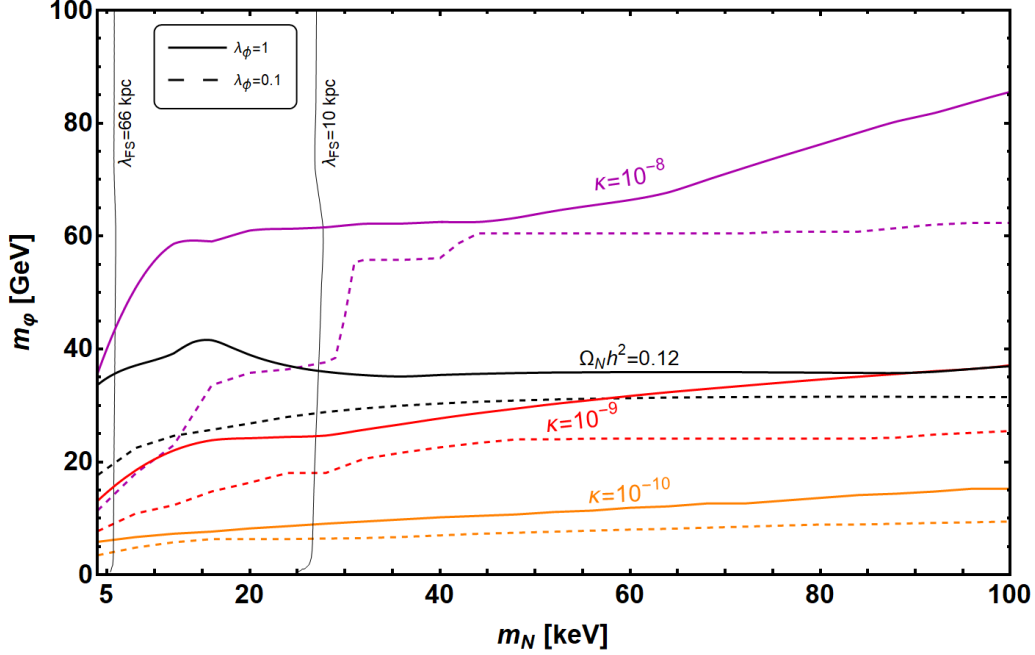


FIG. 7. Thermalisation of the sterile neutrinos. Thermalisation is achieved for values of m_ϕ below the contours. The coloured contours correspond to the given values of κ , the black contours correspond to the value of κ required for $\Omega_N h^2 = 0.12$, which is itself a function of m_ϕ and m_N . The contours of fixed free-streaming horizon are given for the correct relic abundance.

$x \geq 100$ and therefore α follows a Bose-Einstein distribution even when the N relaxation rates fall out of equilibrium at $x \sim 10$.

In Fig. 7 we illustrate the thermalisation as a function of the masses, for different values of κ and λ_ϕ . Thermalisation is achieved below the different contours. Solid contours are for $\lambda_\phi = 1$ and dashed contours for $\lambda_\phi = 0.1$. The purple, red and orange contours correspond to $\kappa = 10^{-8}$, $\kappa = 10^{-9}$ and $\kappa = 10^{-10}$, respectively. For $\lambda_\phi = 0.1$ (dashed contours) the temperature for which thermalisation is achieved is close to the electroweak phase transition and thus the thermalisation is very sensitive to the input parameters. This becomes particularly obvious for $\kappa = 10^{-8}$ (dashed purple contour). For the black contours, κ is fixed by $\Omega_N h^2 = 0.12$. A comparison between the black and the colored curves shows that the correct dark matter abundance requires values of κ that decreases from $\kappa \simeq 10^{-8}$ to $\kappa \simeq 10^{-9}$ as m_N increases for $\lambda_\phi = 1$, and from a few times 10^{-8} to a few times 10^{-9} for $\lambda_\phi = 0.1$. The decreasing κ as m_N increases, for fixed relic abundance, is largely due to the relation $\Omega_N \propto \kappa^{3/2} m_N$ discussed in Sec. IV. For $m_N < 100$ keV, we find that thermalisation of the sterile neutrinos requires reasonably light m_ϕ . Higgs decay is therefore the dominant production mode for most of the parameter space where sterile neutrinos thermalise. Note also that these values of κ and m_ϕ

are consistent with thermalisation of the ϕ sector, cf. Fig. 5. The free-streaming horizons with $\lambda_{\text{FS}} = 10(66)$ kpc are indicated by two almost vertical black contours in Fig. 7. The free-streaming horizon depends on the sterile neutrino mass m_N and the temperature ratio z , as shown in Eqn. (25). The slight deviation from exactly straight contours originates from the z dependence on m_φ , particularly around $m_\varphi \simeq m_h/2$, above which Higgs decay becomes inaccessible as a production mechanism for dark sector particles.

VII. CONCLUSIONS

We have investigated the production of keV sterile neutrino dark matter via a frozen-in complex scalar field. In contrast to the scenario with a real scalar field, the dark sector may thermalise and thus result in a drastically different phenomenology. After the complex scalar field ϕ develops a non-vanishing vacuum expectation value v_ϕ , the sterile neutrinos become massive and the global U(1) symmetry is broken. The dark sector thus consists of the sterile neutrino N , the CP even scalar φ and the pNGB α . Depending on the mass of the φ , the dominant production mechanism of φ is from Higgs decay, scattering or inverse decay.

Subsequently, the pNGB α is produced via φ decay and $\varphi\varphi \rightarrow \alpha\alpha$ scattering. These processes, together with $\alpha\varphi \rightarrow \alpha\varphi$ and $\alpha\alpha \rightarrow \alpha\alpha$, also ensure that the dark scalar sector thermalises for a large region of parameter space, depending on the Higgs portal coupling κ and the quartic dark sector coupling λ_ϕ . Its temperature, T_ϕ , is smaller than the temperature of the SM thermal bath, T . Reproducing the observed DM abundance requires a dark sector temperature ratio $z = T_\phi/T \simeq 0.1$: this puts an upper limit on the mass of the thermalised CP even scalar φ , as shown in Fig. 5. For $m_\varphi < m_h/2$ the dark sector with $z \simeq 0.1$ thermalises easily, even for $\lambda_\phi \sim 10^{-3}$. For heavier φ scalar masses, $m_h/2 < m_\varphi < 2m_h$, the required temperature $z \simeq 0.1$ is close to the thermalisation boundary, indeed whether the sector thermalises depends sensitively on the value of λ_ϕ . Finally, for $m_\varphi > 2m_h$ dark matter will not follow a thermal distribution irrespective of λ_ϕ , assuming the correct relic abundance.

The sterile neutrinos N are produced predominantly via $\varphi \rightarrow NN$ decays and $\alpha\alpha \rightarrow NN$ scattering. The thermalisation of the sterile neutrinos is more difficult to achieve than in the ϕ sector, because the sterile neutrino Yukawa coupling f is small by construction. We find that the thermalisation of this sector generally requires small φ masses and large scalar quartic coupling λ_ϕ . For $m_N < 100$ keV, all of the parameter space in which thermalisation is achieved and the correct relic abundance is produced corresponds to the CP even scalar mass being $m_\varphi < m_h/2$, see Fig. 7. In this case, although the pNGBs and sterile neutrinos modify

the effective number of neutrinos in the early Universe, N_{eff} , their contribution is below the sensitivity of CMB-S4 [41], being $\mathcal{O}(10^{-3})$.

Despite the thermalisation of the ϕ sector and the sterile neutrinos, the influence of the latter on structure formation in this model is similar to other sterile neutrino DM models. Its free-streaming horizon depends mainly on its mass, m_N , and the temperature ratio z , depending only on m_ϕ via z . It agrees with the bound on early-decoupled fermionic DM [42], for which there is a lower limit $m_{\text{DM}} > 5.3$ keV, because the combination of the sterile neutrino mass and the explanation of the observed dark matter abundance fixes the temperature ratio and thus the free-streaming horizon.

In this work, we only considered the case where the dark sector fully thermalises. We would like to stress that the dark sector may not thermalise or only partially thermalise, and thus there is a rich phenomenology to explore which we leave for future work. Thermalisation is not essential to explain the correct dark matter abundance. As illustrated in Fig. 3, the dark sector particle abundances will generally be smaller if they do not thermalise than if they had, therefore a lack of thermalisation could be compensated for by a slightly larger value of κ to produce the right amount of DM. Moreover, we only considered one sterile neutrino N , and thus the $U(1)$ symmetry is anomalous. It is straightforward to make the $U(1)$ symmetry anomaly free by introducing three sterile neutrinos. The additional sterile neutrinos could generate neutrino masses like in the neutrino minimal Standard Model [7].

ACKNOWLEDGMENTS

We thank Michele Frigerio, Karsten Jedamzik, Oleg Sushkov, and Matthew O’Brien for illuminating discussions. R.C. thanks the UNSW School of Physics for its hospitality during part of this project. This project has received support from the IISN convention 4.4503.15 and the Australian Research Council.

Appendices

Appendix A: Self energy of the pNGB

We follow the Kobes-Semenoff [47, 48] formalism to calculate the imaginary part of the pNGB self energy in a thermal background. The relevant 1-loop self-energy diagram is shown

in Fig. 8. Note that the 1-loop diagram with the quartic interaction does not contribute to the imaginary part of the self-energy. We denote the 4-momentum of the pNGB by P^μ , its energy by p_0 and the absolute magnitude of its 3-momentum by p . In the result we have to distinguish between three cases depending on P^2 . For a real on-shell pNGB with $P^2 = 0$ we find

$$\text{Im}\bar{\Pi}(P^2 = 0) = \epsilon(p_0) \frac{m_\varphi^4}{16\pi v_\phi^2 \beta p} \left(\beta p - \ln \left| \frac{f(\frac{m_\varphi^2}{4p})}{f(p + \frac{m_\varphi^2}{4p})} \right| \right), \quad (\text{A1})$$

where $\beta \equiv 1/T$, f is the distribution function, and ϵ is the sign function. For space-like P^2 with $P^2 < 0$ we find

$$\text{Im}\bar{\Pi}(P) = \frac{\epsilon(p_0)}{16\pi v_\phi^2 \beta p} [P^2 - m_\varphi^2]^2 \theta(-P^2) \left[2\beta p - \ln \left| \frac{f(\frac{p_0-p}{2} \frac{m_\varphi^2}{P^2})}{f(p + \frac{p_0-p}{2} \frac{m_\varphi^2}{P^2})} \right| - \ln \left| \frac{f(-\frac{p_0+p}{2} \frac{m_\varphi^2}{P^2})}{f(p - \frac{p_0+p}{2} \frac{m_\varphi^2}{P^2})} \right| \right] \quad (\text{A2})$$

Finally for time-like P^2 with $P^2 > 0$ we have to distinguish whether the energy p_0 is positive or negative. Note that we slightly modified the equations above in order to obtain a more compact expression by introducing absolute magnitudes. We find

$$\begin{aligned} \text{Im}\bar{\Pi}(P) = & \frac{\epsilon(p_0)}{16\pi v_\phi^2 \beta p} [P^2 - m_\varphi^2]^2 \theta(P^2) \\ & \left\{ \theta(P^2 - m_\varphi^2) \left[\ln \left| \frac{f(\frac{p_0+p}{2} + \frac{(p_0-p)}{2} \frac{m_\varphi^2}{P^2})}{f(-\frac{p_0-p}{2} + \frac{p_0-p}{2} \frac{m_\varphi^2}{P^2})} \right| - \ln \left| \frac{f(\frac{p_0-p}{2} + \frac{p_0+p}{2} \frac{m_\varphi^2}{P^2})}{f(-\frac{p_0+p}{2} + \frac{p_0+p}{2} \frac{m_\varphi^2}{P^2})} \right| \right] \right. \\ & + \theta(m_\varphi^2 - P^2) \left[\ln \left| \frac{f(-\frac{p_0+p}{2} + \frac{|p_0|+p}{2} \frac{m_\varphi^2}{P^2})}{f(\frac{p_0-p}{2} + \frac{|p_0|+p}{2} \frac{m_\varphi^2}{P^2})} \right| \right. \\ & \left. \left. - \theta(p_0 - p) \ln \left| \frac{f(-\frac{p_0-p}{2} + \frac{p_0-p}{2} \frac{m_\varphi^2}{P^2})}{f(\frac{p_0+p}{2} + \frac{p_0-p}{2} \frac{m_\varphi^2}{P^2})} \right| - \theta(-p - p_0) \ln \left| \frac{f(\frac{\sqrt{p^2+m_\varphi^2}-p_0}{2})}{f(\frac{\sqrt{p^2+m_\varphi^2}+p_0}{2})} \right| \right] \right\} \end{aligned} \quad (\text{A3})$$

Using the above, we obtain for the propagator of the pNGB α ,

$$D_\alpha(P) = \frac{i}{P^2 - i\text{Im}\bar{\Pi}(P) + i\epsilon}. \quad (\text{A4})$$

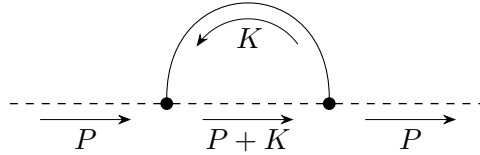


FIG. 8. Relevant contributions to the imaginary part of the self-energy at 1-loop order. Solid lines indicate φ scalar propagators and dashed lines α pNGB propagators.

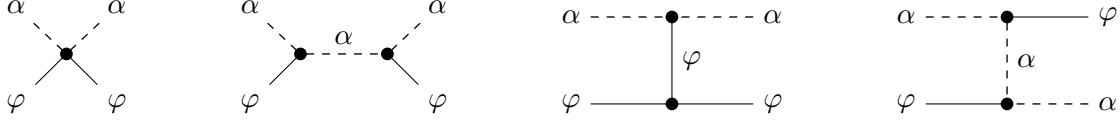


FIG. 9. Contributions to $\alpha\varphi \rightarrow \alpha\varphi$ scattering. Dashed (solid) lines correspond to α (φ) propagators.

Appendix B: $\alpha\varphi \rightarrow \alpha\varphi$ scattering

We discuss the scattering of $\alpha\varphi \rightarrow \alpha\varphi$ in more detail to properly address the u -channel soft-collinear singularity. The relevant Feynman diagrams are given in Fig. 9. We find for the matrix element

$$i\mathcal{M} = -2i\lambda_\phi \left[\frac{t}{m_\varphi^2} + \frac{3t}{t - m_\varphi^2} + \frac{(s - m_\varphi^2)^2}{m_\varphi^2 s} + \frac{(u - m_\varphi^2)^2}{u - i\text{Im}\bar{\Pi}} \right], \quad (\text{B1})$$

in terms of the Mandelstam variables $s = (p_\alpha + p_\varphi)^2$, $t = (p_\alpha - p'_\alpha)^2$, and $u = (p_\alpha - p'_\varphi)^2$. Here p_α (p_φ) denotes the 4-momentum of the incoming α (φ) particles and p'_α (p'_φ) denotes the 4-momentum of the outgoing α (φ) particles. We included the correction from the thermal self energy of α , derived in the previous appendix, for the u -channel diagram to regularise the divergence.⁷ For all other internal propagators, we neglected it as there are no other singularities. We also neglected the φ width for the φ propagator. The self-energy complicates the evaluation of the interaction rate due to its explicit energy dependence. We thus split up the interaction rate into three parts: the u -channel diagram, the other three diagrams, and the interference term.

The u -independent term can be directly evaluated using standard techniques in the centre of mass frame and is given in Eqn. (47). In order to evaluate the u -dependent part, we have to resort to an explicit calculation in a general frame. After evaluating the integral over p'_φ using the delta function, we introduce spherical coordinates and choose the following parameterisation for the 3-momenta,

$$\mathbf{p}_\varphi = p_\varphi(0, 0, 1)^T \quad \mathbf{p}_\alpha = p_\alpha(0, s_x, c_x)^T \quad \mathbf{p}'_\alpha = p'_\alpha(s_\beta s_\theta, c_\beta s_\theta, c_\theta)^T, \quad (\text{B2})$$

where $s_X \equiv \sin X$ and $c_X \equiv \cos X$. Approximating the distribution function by a Maxwell-

⁷The contribution of thermal self energy corrections to the regularisation of t (and u) channel diagrams in cosmology was recently discussed in Ref. [49].

Boltzmann distribution and neglecting statistical factors, we obtain for the interaction rate

$$\langle \Gamma_u \rangle_\varphi = \frac{\lambda_\phi^2 m_\varphi}{8(2\pi)^5 x_\varphi n_\varphi} \int_{m_\varphi}^\infty dE_\varphi \int_{-1}^1 d\cos\theta \left(\int_{-\infty}^0 I_\alpha^- du + \int_0^{m_\varphi^2} I_\alpha^+ du \right) \frac{(m_\varphi^2 - u)^5 p_\varphi f(E_\varphi)}{m_\varphi^4 |u - i\text{Im}\Pi_\alpha|^2 (E_\varphi - p_\varphi \cos\theta)^2 \sqrt{p_\alpha'^2 + p_\varphi^2 - 2p_\alpha' p_\varphi \cos\theta}} \quad (\text{B3})$$

with $|\mathbf{p}'_\alpha - \mathbf{p}_\varphi| = \sqrt{p_\alpha'^2 + p_\varphi^2 - 2p_\varphi p_\alpha' c_\theta}$, the Mandelstam variable $u = m_\varphi^2 - 2p_\alpha' (E_\varphi - p_\varphi c_\theta) \leq m_\varphi^2$ and the two functions I_α^\mp which are non-zero for $u < 0$ and $0 < u < m_\varphi^2$, respectively,

$$I_\alpha^- = \theta(-u) \left[\theta(p_{\alpha-}) \left(e^{-p_{\alpha+}/T} \theta(p_{\alpha+} - p'_\alpha + E_\varphi) + e^{-(p'_\alpha - E_\varphi)/T} \theta(p'_\alpha - E_\varphi - p_{\alpha+}) \right) \right. \\ + (\theta(E_\varphi - p'_\alpha) + e^{-(p'_\alpha - E_\varphi)/T} \theta(p'_\alpha - E_\varphi) - e^{-p_{\alpha+}/T} \theta(p_{\alpha-} - p'_\alpha - E_\varphi)) \\ + \theta(p_{\alpha+}) \theta(-p_{\alpha-}) \left(e^{-p_{\alpha+}/T} \theta(p_{\alpha+} - p'_\alpha + E_\varphi) + e^{-(p'_\alpha - E_\varphi)/T} \theta(p'_\alpha - E_\varphi - p_{\alpha+}) \right) \\ \left. + \theta(-p_{\alpha+}) \left(\theta(E_\varphi - p'_\alpha) + e^{-(p'_\alpha - E_\varphi)/T} \theta(p'_\alpha - E_\varphi) \right) \right] \quad (\text{B4})$$

$$I_\alpha^+ = \theta(u) \theta(m_\varphi^2 - u) \theta(p_{\alpha-} - p'_\alpha + E_\varphi) \left[\theta(p_{\alpha+}) \left(e^{-p_{\alpha+}/T} \theta(p_{\alpha+} - p'_\alpha + E_\varphi) + e^{-(p'_\alpha - E_\varphi)/T} \theta(p'_\alpha - E_\varphi - p_{\alpha+}) \right) \right. \\ \left. + \theta(p_{\alpha-}) \theta(-p_{\alpha+}) \left(\theta(E_\varphi - p'_\alpha) + e^{-(p'_\alpha - E_\varphi)/T} \theta(p'_\alpha - E_\varphi) \right) - e^{-p_{\alpha-}/T} \theta(p_{\alpha-}) \right], \quad (\text{B5})$$

which are defined piecewise and depend on

$$p_{\alpha,\pm} = \frac{u - m_\varphi^2}{2u} [p'_\alpha - E_\varphi \pm |\mathbf{p}'_\alpha - \mathbf{p}_\varphi|] . \quad (\text{B6})$$

Similarly, we obtain for the relevant interaction rate for initial thermalisation using the distribution functions $f_\varphi(E_\varphi) = C_\varphi \delta(E_\varphi - X_\varphi)$ and $f_\alpha(p_\alpha) = C_\alpha \delta(p_\alpha - X_\alpha)$,

$$\langle \Gamma_u \rangle_\varphi = \frac{\lambda_\phi^2 C_\alpha C_\varphi}{8(2\pi)^5 n_\varphi} \int_{-1}^1 d\cos\theta \left(\int_{-\infty}^0 I_\alpha^- du + \int_0^{m_\varphi^2} I_\alpha^+ du \right) \frac{(m_\varphi^2 - u)^5 p_\varphi \theta(X_\varphi - m_\varphi)}{m_\varphi^4 |u - i\text{Im}\Pi_\alpha|^2 (X_\varphi - p_\varphi \cos\theta)^2 \sqrt{p_\alpha'^2 + p_\varphi^2 - 2p_\alpha' p_\varphi \cos\theta}} , \quad (\text{B7})$$

with $p_\varphi \equiv \sqrt{X_\varphi^2 - m_\varphi^2}$ and the two piecewise defined functions

$$\begin{aligned}
I_\alpha^- = \theta(-u) & \left[\theta(p_{\alpha-}) \left(\theta(X_\alpha - p_{\alpha+}) \theta(p_{\alpha+} - p'_\alpha + X_\varphi) + \theta(X_\alpha - (p'_\alpha - X_\varphi)) \theta(p'_\alpha - X_\varphi - p_{\alpha+}) \right) \right. \\
& + (\theta(X_\varphi - p'_\alpha) + \theta(X_\alpha - (p'_\alpha - X_\varphi)) \theta(p'_\alpha - X_\varphi) - \theta(p_{\alpha+} - X_\alpha)) \theta(p_{\alpha-} - p'_\alpha - X_\varphi) \\
& + \theta(p_{\alpha+}) \theta(-p_{\alpha-}) \left(\theta(X_\alpha - p_{\alpha+}) \theta(p_{\alpha+} - p'_\alpha + X_\varphi) + \theta(X_\alpha - (p'_\alpha - X_\varphi)) \theta(p'_\alpha - X_\varphi - p_{\alpha+}) \right) \\
& \left. + \theta(-p_{\alpha+}) \left(\theta(X_\varphi - p'_\alpha) + \theta(X_\alpha - (p'_\alpha - X_\varphi)) \theta(p'_\alpha - X_\varphi) \right) \right], \tag{B8}
\end{aligned}$$

$$\begin{aligned}
I_\alpha^+ = \theta(u) \theta(m_\varphi^2 - u) \theta(p_{\alpha-} - p'_\alpha + X_\varphi) & \left[\right. \tag{B9} \\
& \theta(p_{\alpha+}) \left(\theta(X_\alpha - p_{\alpha+}) \theta(p_{\alpha+} - p'_\alpha + X_\varphi) + \theta(X_\alpha - (p'_\alpha - X_\varphi)) \theta(p'_\alpha - X_\varphi - p_{\alpha+}) \right) \\
& \left. + \theta(p_{\alpha-}) \theta(-p_{\alpha+}) \left(\theta(X_\varphi - p'_\alpha) + \theta(X_\alpha - (p'_\alpha - X_\varphi)) \theta(p'_\alpha - X_\varphi) \right) - \theta(p_{\alpha-} - X_\alpha) \theta(p_{\alpha-}) \right].
\end{aligned}$$

Using the Cuba library [50], we numerically find that the u -channel contribution is generally subdominant for the parameter region of interest with a few exceptions, where it becomes of the same order of magnitude as the u -independent part. In the main part of the text we hence neglect the u -channel contribution and the interference term in order to reduce the computational complexity involved with evaluating the multi-dimensional integral for the u -dependent contributions.

-
- [1] N. Aghanim *et al.* (Planck), *Astron. Astrophys.* **641**, A6 (2020), [arXiv:1807.06209 \[astro-ph.CO\]](#).
 - [2] S. Dodelson and L. M. Widrow, *Phys. Rev. Lett.* **72**, 17 (1994), [arXiv:hep-ph/9303287](#).
 - [3] P. Minkowski, *Phys. Lett.* **B67**, 421 (1977).
 - [4] T. Yanagida, *Conf. Proc.* **C7902131**, 95 (1979).
 - [5] M. Gell-Mann, P. Ramond, and R. Slansky, *Supergravity Workshop Stony Brook, New York, September 27-28, 1979*, *Conf. Proc.* **C790927**, 315 (1979), [arXiv:1306.4669 \[hep-th\]](#).
 - [6] R. N. Mohapatra and G. Senjanović, *Phys. Rev. Lett.* **44**, 912 (1980).
 - [7] T. Asaka, S. Blanchet, and M. Shaposhnikov, *Phys. Lett. B* **631**, 151 (2005), [arXiv:hep-ph/0503065](#).
 - [8] J. S. Bullock and M. Boylan-Kolchin, *Ann. Rev. Astron. Astrophys.* **55**, 343 (2017), [arXiv:1707.04256 \[astro-ph.CO\]](#).
 - [9] E. Bulbul, M. Markevitch, A. Foster, R. K. Smith, M. Loewenstein, and S. W. Randall, *Astrophys. J.* **789**, 13 (2014), [arXiv:1402.2301 \[astro-ph.CO\]](#).

- [10] A. Boyarsky, O. Ruchayskiy, D. Iakubovskiy, and J. Franse, *Phys. Rev. Lett.* **113**, 251301 (2014), [arXiv:1402.4119 \[astro-ph.CO\]](#).
- [11] S. Tremaine and J. E. Gunn, *Phys. Rev. Lett.* **42**, 407 (1979).
- [12] S. Horiuchi, P. J. Humphrey, J. Onorbe, K. N. Abazajian, M. Kaplinghat, and S. Garrison-Kimmel, *Phys. Rev. D* **89**, 025017 (2014), [arXiv:1311.0282 \[astro-ph.CO\]](#).
- [13] B. W. Lee and S. Weinberg, *Phys. Rev. Lett.* **39**, 165 (1977).
- [14] J. McDonald, *Phys. Rev. Lett.* **88**, 091304 (2002), [arXiv:hep-ph/0106249 \[hep-ph\]](#).
- [15] L. J. Hall, K. Jedamzik, J. March-Russell, and S. M. West, *JHEP* **03**, 080 (2010), [arXiv:0911.1120 \[hep-ph\]](#).
- [16] R. Barbieri and A. Dolgov, *Nucl. Phys. B* **349**, 743 (1991).
- [17] K. Enqvist, K. Kainulainen, and J. Maalampi, *Nucl. Phys. B* **349**, 754 (1991).
- [18] A. Boyarsky, J. Lesgourgues, O. Ruchayskiy, and M. Viel, *JCAP* **0905**, 012 (2009), [arXiv:0812.0010 \[astro-ph\]](#).
- [19] X.-D. Shi and G. M. Fuller, *Phys. Rev. Lett.* **82**, 2832 (1999), [arXiv:astro-ph/9810076](#).
- [20] M. Shaposhnikov and I. Tkachev, *Phys. Lett. B* **639**, 414 (2006), [arXiv:hep-ph/0604236 \[hep-ph\]](#).
- [21] A. Kusenko, *Phys. Rev. Lett.* **97**, 241301 (2006), [arXiv:hep-ph/0609081](#).
- [22] K. Petraki and A. Kusenko, *Phys. Rev. D* **77**, 065014 (2008), [arXiv:0711.4646 \[hep-ph\]](#).
- [23] D. Boyanovsky, *Phys. Rev. D* **78**, 103505 (2008), [arXiv:0807.0646 \[astro-ph\]](#).
- [24] A. Merle, *Int. J. Mod. Phys. D* **22**, 1330020 (2013), [arXiv:1302.2625 \[hep-ph\]](#).
- [25] A. Merle, V. Niro, and D. Schmidt, *JCAP* **03**, 028 (2014), [arXiv:1306.3996 \[hep-ph\]](#).
- [26] M. Frigerio and C. E. Yaguna, *Eur. Phys. J. C* **75**, 31 (2015), [arXiv:1409.0659 \[hep-ph\]](#).
- [27] A. Adulpravitchai and M. A. Schmidt, *JHEP* **01**, 006 (2015), [arXiv:1409.4330 \[hep-ph\]](#).
- [28] Z. Kang, *Eur. Phys. J. C* **75**, 471 (2015), [arXiv:1411.2773 \[hep-ph\]](#).
- [29] A. Merle and M. Totzauer, *JCAP* **06**, 011 (2015), [arXiv:1502.01011 \[hep-ph\]](#).
- [30] A. Adulpravitchai and M. A. Schmidt, *JHEP* **12**, 023 (2015), [arXiv:1507.05694 \[hep-ph\]](#).
- [31] V. De Romeri, D. Karamitros, O. Lebedev, and T. Toma, *JHEP* **10**, 137 (2020), [arXiv:2003.12606 \[hep-ph\]](#).
- [32] Y. B. Zeldovich, I. Y. Kobzarev, and L. B. Okun, *Zh. Eksp. Teor. Fiz.* **67**, 3 (1974).
- [33] R. Coy, T. Hambye, M. H. G. Tytgat, and L. Vanderheyden, *Phys. Rev. D* **104**, 055021 (2021), [arXiv:2105.01263 \[hep-ph\]](#).
- [34] N. Fernandez, Y. Kahn, and J. Shelton, (2021), [arXiv:2111.13709 \[hep-ph\]](#).
- [35] G. 't Hooft, *Recent Developments in Gauge Theories. Proceedings, Nato Advanced Study Institute, Cargese, France, August 26 - September 8, 1979*, *NATO Sci. Ser. B* **59**, 135 (1980).
- [36] T. Hambye, M. H. G. Tytgat, J. Vandecasteele, and L. Vanderheyden, *Phys. Rev. D* **100**, 095018 (2019), [arXiv:1908.09864 \[hep-ph\]](#).
- [37] M. Drewes *et al.*, *JCAP* **01**, 025 (2017), [arXiv:1602.04816 \[hep-ph\]](#).
- [38] R. Foot, A. Kobakhidze, K. L. McDonald, and R. R. Volkas, *Phys. Rev. D* **89**, 115018 (2014), [arXiv:1310.0223 \[hep-ph\]](#).

- [39] D. J. E. Marsh, *Phys. Rept.* **643**, 1 (2016), [arXiv:1510.07633 \[astro-ph.CO\]](#).
- [40] M. D’Onofrio and K. Rummukainen, *Phys. Rev. D* **93**, 025003 (2016), [arXiv:1508.07161 \[hep-ph\]](#).
- [41] K. N. Abazajian *et al.* (CMB-S4), (2016), [arXiv:1610.02743 \[astro-ph.CO\]](#).
- [42] V. Iršič *et al.*, *Phys. Rev. D* **96**, 023522 (2017), [arXiv:1702.01764 \[astro-ph.CO\]](#).
- [43] O. Wantz and E. Shellard, *Phys.Rev.* **D82**, 123508 (2010), [arXiv:0910.1066 \[astro-ph.CO\]](#).
- [44] S. Hofmann, D. J. Schwarz, and H. Stoecker, *Phys. Rev.* **D64**, 083507 (2001), [arXiv:astro-ph/0104173 \[astro-ph\]](#).
- [45] G. Arcadi, O. Lebedev, S. Pokorski, and T. Toma, *JHEP* **08**, 050 (2019), [arXiv:1906.07659 \[hep-ph\]](#).
- [46] G. Giudice, A. Notari, M. Raidal, A. Riotto, and A. Strumia, *Nucl. Phys. B* **685**, 89 (2004), [arXiv:hep-ph/0310123](#).
- [47] R. Kobes and G. Semenoff, *Nucl. Phys. B* **260**, 714 (1985).
- [48] R. Kobes and G. Semenoff, *Nucl. Phys. B* **272**, 329 (1986).
- [49] B. Grzadkowski, M. Iglicki, and S. Mrówczyński, (2021), [arXiv:2108.01757 \[hep-ph\]](#).
- [50] T. Hahn, *Comput. Phys. Commun.* **168**, 78 (2005), [arXiv:hep-ph/0404043](#).